Neurobiology of Disease

Gene Expression Analyses Identify Narp Contribution in the Development of L-DOPA-Induced Dyskinesia

Fanny Charbonnier-Beaupel,[1,2,3,4]* Marion Malerbi,[1,2,3,5,6]* Cristina Alcacer,[1,5,6]* Khadija Tahiri,[1,2,3] Wassila Carpentier,[7] Chuansong Wang,[8] Matthew During,[8] Desheng Xu,[9] Paul F. Worley,[9] Jean-Antoine Girault,[1,5,6] Denis Hervé,[1,5,6]* and Jean-Christophe Corvol[1,2,3,10]*

[1]Sorbonne Universités, UPMC Univ Paris 06, Paris, France, [2]Inserm, UMR-S 1127, ICM, Pitié-Salpêtrière Hospital, 75013 Paris, France, [3]CNRS, UMR 7225, 75013 Paris, France, [4]Assistance Publique Hôpitaux de Paris, Department of Pharmacy, Pitié-Salpêtrière Hospital, 75013 Paris, France, [5]Inserm UMR-S 839, 75005 Paris, France, [6]Institut du Fer à Moulin, 75005 Paris, France, [7]UPMC Univ Paris 06, Post genomic platform P3S, 75013 Paris, France, [8]Departments of Molecular Virology, Immunology and Medical Genetics, Neuroscience and Neurological Surgery, The Ohio State University, Columbus, Ohio 43210, [9]Johns Hopkins University School of Medicine, Solomon H. Snyder Department of Neuroscience, Baltimore, Maryland 21205, and [10]Assistance Publique Hôpitaux de Paris, Inserm, Clinical Investigation Center, CIC-1422, Pitié-Salpêtrière Hospital, 75013 Paris, France

In Parkinson's disease, long-term dopamine replacement therapy is complicated by the appearance of L-DOPA-induced dyskinesia (LID). One major hypothesis is that LID results from an aberrant transcriptional program in striatal neurons induced by L-DOPA and triggered by the activation of ERK. To identify these genes, we performed transcriptome analyses in the striatum in 6-hydroxydopamine-lesioned mice. A time course analysis (0–6 h after treatment with L-DOPA) identified an acute signature of 709 genes, among which genes involved in protein phosphatase activity were overrepresented, suggesting a negative feedback on ERK activation by L-DOPA. L-DOPA-dependent deregulation of 28 genes was blocked by pretreatment with SL327, an inhibitor of ERK activation, and 26 genes were found differentially expressed between highly and weakly dyskinetic animals after treatment with L-DOPA. The intersection list identified five genes: *FosB*, *Th*, *Nptx2*, *Nedd4l*, and *Ccrn4l*. *Nptx2* encodes neuronal pentraxin II (or neuronal activity-regulated pentraxin, Narp), which is involved in the clustering of glutamate receptors. We confirmed increased *Nptx2* expression after L-DOPA and its blockade by SL327 using quantitative RT-PCR in independent experiments. Using an escalating L-DOPA dose protocol, LID severity was decreased in Narp knock-out mice compared with their wild-type littermates or after overexpression of a dominant-negative form of Narp in the striatum. In conclusion, we have identified a molecular signature induced by L-DOPA in the dopamine-denervated striatum that is dependent on ERK and associated with LID. Here, we demonstrate the implication of one of these genes, *Nptx2*, in the development of LID.

Key words: **L-DOPA-induced dyskinesia; Narp; Parkinson's disease; transcriptome**

Introduction

In Parkinson's disease (PD), motor symptoms are mainly caused by degeneration of dopaminergic neurons from the substantia nigra pars compacta projecting to the dorsal striatum. Although dopamine replacement therapy by L-DOPA remains the most widely used treatment of motor symptoms, it is complicated by the development of abnormal involuntary movements (AIMs) called L-DOPA-induced dyskinesia (LID; Duvoisin, 1974). Converging evidence suggests that LID results from aberrant neuroplasticity triggered by the repeated stimulation of "sensitized" dopamine receptors (Obeso et al., 2000; Jenner, 2008).

Dopamine controls long-term potentiation and depression (LTP and LTD) of corticostriatal synapses (Shen et al., 2008) in medium-sized spiny striatal neurons (MSNs), which express either D1 or D2 dopamine receptors (D1R or D2R, respectively; Gerfen et al., 1990). Corticostriatal plasticity is altered in animal models of PD and is rescued by chronic L-DOPA treatment (Calabresi et al., 2007; Kreitzer and Malenka, 2007). Dyskinetic animals selectively display a loss of LTP depotentiation after low-frequency stimulation of afferents, an effect resulting from D1R signaling sensitization (Picconi et al., 2003). D1R signaling is enhanced in the striatum after dopamine denervation in animal models and in patients with PD (Hervé et al., 1993; Corvol et al., 2004; Aubert et al., 2005; Westin et al., 2007, Santini, 2009a; Lebel et al., 2010; Rangel-Barajas et al., 2011; Alcacer et al., 2012). Phar-

Received Dec. 8, 2013; revised Nov. 1, 2014; accepted Nov. 5, 2014.

Author contributions: F.C.-B., M.M., C.A., J.-A.G., D.H., and J.-C.C. designed research; F.C.-B., M.M., C.A., K.T., W.C., C.W., M.D., D.X., D.H., and J.-C.C. performed research; P.F.W. contributed unpublished reagents/analytic tools; F.C.-B., M.M., K.T., and J.-C.C. analyzed data; F.C.-B., M.M., C.A., K.T., W.C., C.W., M.D., D.X., P.F.W., J.-A.G., D.H., and J.-C.C. wrote the paper.

The work was supported by the University Pierre and Marie Curie (UPMC), Inserm (Grant Inserm/DHOS 2008), the Fondation pour la Recherche Médicale, the Société française de pharmacologie et de thérapeutique, the Agence Nationale de la Recherche (Grant ANR09-MNPS-014), the Michael Stern Parkinson's Research Foundation, and the European Research Council. The research leading to these results has received funding from the program "Investissements d'avenir" ANR-10-IAIHU-06. P.W. was supported by National Institutes of Health Grant R01 NS039156.; We thank the staff of the Institut du Fer a Moulin Imaging and animal facilities and the staff of the Plateforme post-genomique P3S facility at the Pitié-Salpêtrière Hospital. Analyses were performed using Biometric Research Branch ArrayTools developed by Dr. Richard Simon and BRB-ArrayTools Development Team.

The authors declare no competing financial interests.

*F.C.-B., M.M., C.A., D.H., and J.-C.C. contributed equally to this work.

Correspondence should be addressed to Dr. Jean-Christophe CORVOL, ICM, Hôpital de la Pitié-Salpêtrière, 47 Bd de l'Hôpital, 75651 Paris Cedex 13, France. E-mail: jean-christophe.corvol@psl.aphp.fr.

DOI:10.1523/JNEUROSCI.5231-13.2015

 0270-6474/15/350096-16$15.00/0

macological blockade of D1R, or its genetic ablation, reduces the intensity of LID in animals (Westin et al., 2007; Darmopil et al., 2009). Stimulation of D1R and NMDA glutamate receptors can activate signaling cascades involving cAMP-dependent protein kinase (PKA), dopamine- and cAMP-regulated phosphoprotein of 32 kDa (DARPP-32), and ERK in D1R-expressing MSNs (Valjent et al., 2005). In 6-OHDA-lesioned animals, administration of L-DOPA activates a D1R-dependent Ras-ERK signaling pathway (Gerfen et al., 2002; Westin et al., 2007) that is correlated with the intensity of LID (Schuster et al., 2008; Darmopil et al., 2009; Lindgren et al., 2009; Santini et al., 2009a; Santini et al., 2009b; Lebel et al., 2010; Santini et al., 2010; Francardo et al., 2011). LID is blocked or decreased by pharmacological or genetic inhibition of the ERK pathway (Santini et al., 2007; Fasano et al., 2010). However, the activation of ERK is intense after the first L-DOPA treatment but tends to fade with chronic treatments, even in dyskinetic animals (Santini et al., 2007; Ding et al., 2011). In contrast, the intensity of LID is increased or maintained by repetition of L-DOPA administrations (Lundblad et al., 2005). This suggests that the initial activation of ERK-dependent signaling cascades primes long-lasting changes in the striatal neuronal networks that maintain LID after prolonged treatment (Cenci et al., 2010). These changes could involve gene transcription, a major ERK target, as illustrated by the L-DOPA-induced expression of ΔFosB that contributes to LID development and maintenance (Andersson et al., 1999; Andersson et al., 2003; Berton et al., 2009; Cao et al., 2010). However, the early patterns of gene expression implicated in LID remain largely unknown. We hypothesized that very early ERK-dependent changes in gene expression play a key role in the later appearance of striatal dysfunction revealed by LID. We therefore investigated ERK-dependent gene expression changes induced by the first administration of L-DOPA and associated with the early development of abnormal involuntary movements in unilaterally 6-OHDA-lesioned mice. Using this strategy, we identified neuronal activity-regulated pentraxin (Narp) as an ERK-dependent gene induced by L-DOPA and showed a decrease of LID in Narp knock-out (KO) mice or after overexpression of the dominant-negative form of Narp in the striatum.

Materials and Methods

Animals

Eight-week-old C57BL/6J mice were maintained in a 12 h light/dark cycle in stable conditions of temperature (22°C) with access to food and water *ad libitum*. All experiments were conducted in accordance with the guidelines of the French Agriculture and Forestry Ministry for handling animals (Decree 87-848) and under the approval of the Direction Départementale de la Protection des Populations de Paris (Authorization C-75-828, License B75-05-22). Generation of Narp KO mice has been described previously (Bjartmar et al., 2006). Narp KO and wild-type (WT) control mice were obtained by breeding Narp heterozygotes. Both male and female WT and KO mice were used and their age was 10–11 weeks at the start of lesion.

6-OHDA lesions, AAV injections, and postoperative care

Mice were anesthetized with a mixture of xylazine (10 mg/ml) and pentobarbital (25 mg/ml; Centravet) and mounted in a digitalized stereotaxic frame (Stoelting) equipped with a mouse adaptor. 6-OHDA-HCl (3.0 mg/ml; Sigma-Aldrich) was dissolved in a solution containing 0.2 g/L ascorbic acid and 9 g/L NaCl. Mice were lesioned as described previously (Alcacer et al., 2012) by receiving two unilateral injections (2 × 2 μl) of 6-OHDA into the right striatum at the following coordinates according to the mouse brain atlas (Paxinos and Franklin, 2001): anteroposterior, +1.2 mm; lateral, +2.1 mm; dorsoventral, −3.2 mm; and anteroposterior, +0.6 mm; lateral, +2.4 mm; dorsoventral, −3.2 mm. A Narp construct that acts as a dominant negative for WT Narp secretion (Narp-N13; Δ345–416), as well as a Narp deletion construct that does not inhibit WT Narp secretion (Narp-N; Δ191–410; O'Brien et al., 2002) were used to generate adeno-associated virus (AAV) expression constructs as described previously (During et al., 2003). For the AAV experiment, 6-OHDA (12 μg/μl) and AAV (AAV-DN13: 3.5×10^{13} vg/ml; AAV-Narp-N: 2.2×10^{13} vg/ml; AAV-eGFP 3.34×10^{13} vg/ml) were injected into the right striatum (1 injection, 2 μl) at the following coordinates according to the mouse brain atlas (Paxinos and Franklin, 2001): anteroposterieur, +0.4 mm; lateral, +2 mm; dorsoventral, −3 mm. Each injection was performed with a 36-gauge, 50-mm-long stainless steel cannula connected to a syringe pump (MTI Corporation) by a polyethylene catheter, at a slow rate of 0.25 μl/min to minimize tissue damage. After the injection, the cannula was left in place for additional 4 min before being slowly retracted. Mice were left on a warm plate for ~24 h after surgery to avoid hypothermia. To reduce suffering, mice received subcutaneous injections of a nonsteroidal anti-inflammatory drug (flunixin meglumine, 4 mg/kg; Sigma-Aldrich) just after the surgery and twice daily for 2 d after surgery. Mice were allowed to recover for 4 weeks before behavioral evaluation and drug treatment. Dopaminergic depletion in the striatum was assessed by determining the striatal levels of tyrosine hydroxylase (TH) by immunoblotting.

Treatments

L-DOPA and the peripheral DOPA decarboxylase inhibitor benserazide hydrochloride (Sigma-Aldrich) were dissolved together in physiological saline solution (9 g/L NaCl). In the acute experiments, L-DOPA and benserazide hydrochloride were injected intraperitoneally at a dose of 20 and 12 mg/kg, respectively, in a volume of 10 ml/kg body weight. α-[amino[(4-aminophenyl)thio]methylene]-2-(trifluoromethyl)benzeneacetonitrile (SL327; Sigma-Aldrich) was dissolved in DMSO diluted twice in water (final concentration of DMSO, 50%) and injected intraperitoneally (50 mg/kg; 2 ml/kg) 30 min before injection of L-DOPA. Control mice received the same injection of diluted DMSO without SL327 (vehicle). In the subchronic experiment, mice were treated for 2 d with L-DOPA (20 mg/kg) and benserazide hydrochloride (12 mg/kg) or vehicle separated by a 24 h interval. Narp KO mice, WT littermates, and AAV-injected mice were treated chronically with L-DOPA and benserazide using an escalating dose protocol (5, 10, and 20 mg/kg L-DOPA, i.p., daily for 5 d for each dose, the benserazide dose remaining fixed at 12 mg/kg). Mice were killed by decapitation.

Behavioral tests

Cylinder test. The sensorimotor function deficit was evaluated in the cylinder test to estimate Parkinsonism in the various lesioned mice (Lundblad et al., 2002). Mice were placed one by one in glass cylinders and video recorded for 5 min without previous habituation to the glass cylinder. Once introduced into the cylinder, the mice showed an exploratory behavior reflected by rearing and forepaw contacts on the wall. The number of contacts with the right or left forepaw was counted (only contacts in which the animal supported its body weight on the paw with extended digits). The use of the impaired (left) forepaw was expressed as a percentage of the total number of contacts on the wall.

Abnormal involuntary movement. AIMs were assessed using a previously validated scale for scoring LID in mouse (Lundblad et al., 2004, 2005). Immediately after the L-DOPA administration, mice were placed in separate cages and abnormal movements were assessed for 1 min every 20 min over a period of 120 min. Abnormal movements, clearly distinct from natural stereotyped behaviors, were classified into four different subtypes: locomotive (tight contralateral turns), axial (contralateral dystonic posture of the neck and upper body), limb (jerky and fluttering movements of the limb contralateral to the side of the lesion), and orofacial (vacuous jaw movements and tongue protrusions) AIMs. Each subtype was scored on a severity scale from 0 to 4 where 0 = absent, 1 = occasional, 2 = frequent, 3 = continuous, and 4 = continuous and not interruptible by external stimuli. A composite axial, limb, and orofacial (ALO) dyskinesia score was obtained by the addition of scores for axial, limb, and orofacial AIMs. To identify the extreme behaviors in the subchronic experiment, highly and weakly dyskinetic mice were separated by

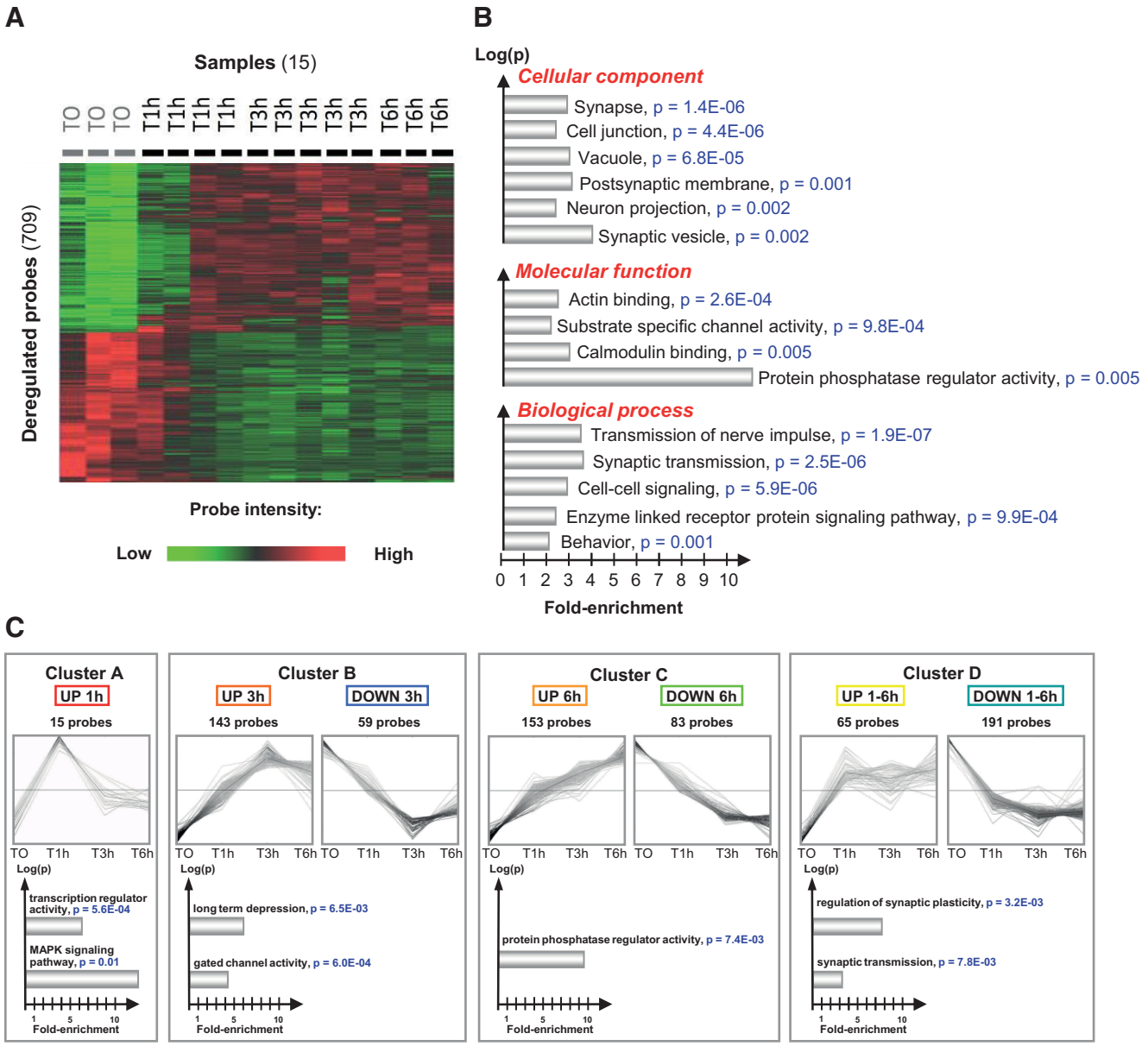

Figure 1. Gene expression signature in the 6-OHDA-denervated striatum after an acute L-DOPA administration. ***A***, Hierarchical clustering (individual data) performed on the 709 probes significantly deregulated after an acute L-DOPA administration (fold change >1.2, $p<0.01$, FDR <0.1). Fifteen samples were analyzed in this experiment (T0, $n=3$; T1h, $n=4$; T3h, $n=5$; T6h, $n=3$). The clustering image was obtained using average dot product distance metric selection and average linkage clustering methods with Multi Experiment Viewer software. The green probes correspond to downregulated genes and red ones correspond to upregulated genes. ***B***, Nonredundant gene ontology analysis (molecular functions, biological process, and cellular components) of the 709 probes list. The analysis was conducted using the functional annotation tool of the David Bioinformation database. Gene ontology pathways with >3 genes were considered significant if fold enrichment was >2-fold and the modified Fisher exact p-value was <0.01. ***C***, Identification of four gene clusters corresponding to the different temporal expression profiles of the 709 probes. The name of genes in each cluster is specified in the Table 1. The data were obtained using an unbiased self-organizing tree algorithm (Pearson correlation in SOTA, Multi Experiment Viewer software). For each cluster, the top shows the time course during the L-DOPA challenge and the bottom shows the results of gene ontology analysis (performed as for ***B***).

a quartile analysis based on ALO score. For the Narp KO mice experiment, assessments were performed in blind conditions by a rater ignoring the mouse genotype.

RNA processing

At the corresponding time points, mice were killed and the striata were dissected with a standardized frozen-based procedure to avoid RNA degradation. After decapitation and dissection, the brain of mice were rapidly frozen by immersion for 1 min in isopentane maintained at −30°C in dry ice. Coronal sections (210 μm thick) were cut with a cryostat and microdisks of striatum were dissected. The samples were stored at −80°C until RNA extraction processing. Total mRNA was extracted using the RNeasyMiniKit (Qiagen) according to the manufacturer's procedure and further controlled for RNA quality (Bioanalyser 2100; Agilent). Next, total mRNA was amplified, labeled (Illumina TotalPrep RNA Amplification Kit; Ambion), and hybridized on Illumina Mouse WG-6v3.0 bead chips (>43 000 probes) at the P3S facility using Illumina's protocol. The Beadchips were scanned on an Illumina IScan with Illumina IScan image data acquisition software (www.illumina.com). To avoid batch effects, sample order processing was randomized. Biological replicate samples of 250 ng of total RNA were reverse transcribed at 25°C for 10 min, 37°C for 2 h, and 85°C for 5 min in a 20 μl reaction buffer according to manufacturer's instructions. Quantification of mRNAs was performed by real-time RT-PCR using a Roche LightCycler LC480 sequence detection system. Oligonucleotide primer pairs were obtained from

Table 1. List of genes significantly deregulated after an acute challenge of L-DOPA

Cluster A	Cluster B						
Peaked 1 h (UP)	Peaked 3 h (UP)					Peaked 3 h (DOWN)	
Egr4	Per2	Nedd4l	**Ppp2r2d**	Caskin2	Erlin1	Tax1bp3	Vstm2a
Egr2	Slc32a1	Fkbp5	Pkp2	Atp2a2	D430042O09Rik	C2cd4c	Fam113a
Per1	Vgf	Prosapip1	Ddit4l	Vti1b	Cdc42ep3	BC046404	Insc
Per1	Gas7	**Cacna1 h**	Abi2	A930005I04Rik	Ndufa8	Tmem141	Epha5
Npas4	AI464131	Ece1	Zfp280d	Ppapdc2	Eif4ebp2	Pgpep1	Fcgrt
Mfap3	**Arpp21**	Csmd3	Smug1	2700062C07Rik	Rit2	Chrm2	Sypl
Dusp1	Crym	Ntrk3	C8b	Ubxn6	**Cacna2d3**	Tax1bp3	Mela
Junb	Spry3	1110018G07Rik	Cinp	Wrb	Ccnyl1	**Araf**	Nfatc3
Arc	Syt4	Sbk1	Rerg	Sez6	Zcchc12	Hexb	Abca7
Fos	Vdac1	Car12	Zfp385b	Spag6	Foxp1	Ctsb	Pgpep1
FosB	Nrarp	Kcnd2	Itgb1bp1	Rab15	**Nptx2**	Rab8a	F11r
Dusp6	Doc2b	Gabarapl1	Kdm4b	Kcnab1	Gng7	Trappc1	Wwtr1
Frat2	Camk1g	Zeb1	**Homer1**	Ippk	Nit1	Vangl2	Eif6
Dusp6	Fam184b	Slc25a44	Vdac1	Mbp	Lmtk2	Vtn	Gns
Nab2	Gdnf	Dmkn	Fdps	Chat	Foxo1	Lpar4	Syt12
	Ppp3r1	Hpca	Ndufa5	Sc4 mol	Astn1	Tusc1	Fam125a
	Pard6a	Nsg2	Capn10	1810046J19Rik	Mpp6	Tpm2	Sp7
	Gnb5	Abi2	Gne	Tmem41b	Psmc3ip	Lpar4	Trib3
	Taf9b	Ido1	Zmynd8	Unc119b	Prpf18	Cmtm8	Fam3a
	Dgkb	Gabrb3	Ncor1	1110017D15Rik	Tiam2	41161	Tex261
	Gria2	Ajap1	Csrnp3	Sf3a1	Dmkn	9130019O22Rik	Naprt1
	Kcnab1	Clic6	Zfhx3	Dcaf4	Nphp4	3632451O06Rik	Slc2a6
	Shank3	Slc2a1	Pfkp	2610034M16Rik	**Grid2**	Apba2	2810474O19Rik
	Nt5e	Dctn3	Reln	Kcnk1		Ifnar2	Tmc6
	Per2	Agfg2	Dnajc2	Banf1		Egfl7	2210016L21Rik
	Fam132a	Atg16l1	Pde4dip	Tdrkh		Fam114a1	Add3
	Tiam1	Mat2a	Pitpnm3	Slc22a17		Cdc42ep2	Pdgfa
	Nt5e	Ubfd1	4833424O15Rik	**Prkg2**		Plekho2	Lor
	Gucy1a3	Tmem70	**Rem2**	Kdm5b		Gkap1	Rnf135
	Kcna5	Pptc7	Ccrn4l	Fem1b		Lgals8	

Cluster C							
Peaked 6 h (UP)					Peaked 6 h (DOWN)		
Lrrc1	Znrf1	**Ppp1cc**	Rgs14	Sfxn3	Sncb	Nav1	Cln6
Unc13c	Zfp930	Casz1	Rundc3b	Cyld	Aspscr1	Plekha2	Acta2
Ino80e	Nsg2	Sh3bgrl3	Ylpm1	Rhobtb2	Tpd52	Psap	Serac1
Mfsd2a	Slmap	Hs6st2	Slc2a13	Chst11	Hdac7	Vamp1	Rfc2
Pdzd2	H2afx	C1galt1c1	Tac1	1110057K04Rik	Triobp	Metap1d	Adck4
Syne1	Ecel1	Vldlr	Slc10a4	Tmem199	Tmem141	Skap1	BC017647
Rap1gap	**Ppp2r2a**	**Ppp2r2c**	Penk	Grb10	Aifm2	Nol3	Pld4
Th	Dazl	Krt10	Srm	Tle1	Ptprd	Nos1ap	Tmed10
Clip4	Vldlr	Sorcs2	Eps15l1	Rhobtb2	Ldb2	Ptbp1	Ccs
Pcsk2	Musk	Arg2	Ptk2b	Crtc1	Reep3	Tcf4	Ednrb
Gpr158	Lypd1	Gpd1	Ubl3	Dab1	Rab3d	Wipf1	2310003H01Rik
Lingo3	Adra2c	Epb4.9	Mterfd3	Ets2	Tmem106c	Npm3	Sepn1
Spock3	Myo5b	Amigo2	Rhbdl3	Bahd1	Tmc6	Klf6	Psap
Trnp1	Mbnl2	4933424B01Rik	Slc25a14	Wdr37	Ptprd	Nol3	Kcna6
Smpd3	1110003E01Rik	Abi1	Sdr39u1	**Cacnb2**	Cmtm4	Vat1	Hcls1
Onecut2	Cxx1c	**Rasgrp1**	Vldlr	Mbnl2	Alpl	Abhd14b	Kcne1l
Cyp2c44	Gpr158	Ddost	Strn	Mdga2	Golim4	Fam189a1	Fam126a
Rarb	C030019I05Rik	Lrrtm3	Slc2a13	Pcdhgb4	Fah	Tnfaip1	Fam105b
Dlg2	Jph3	Sub1	Fnip1	Kdm3a	Glb1	Ptbp1	Btbd3
Arpp19	Rilp	Ccng2	Ncbp1	Spink8	Pinx1	Gpd2	Dcakd
Ppp1r2	Dgki	Trpc3	Ndufs4	Fbll1	1700084C01Rik	Fchsd1	Gm4671
Gdf10	Tmcc2	Pkia	Dixdc1	Rilpl1	Slc6a7	Padi2	
Trerf1	Mxd1	Vat1l	Zfp758	Ube3c	Sox9	Skp2	
Ppp4r4	Dlk1	Coch	Zfp39	Tmem49	Slc38a2	Nol3	
Ramp1	Gps1	Wdr17	Mtf2	Cyp2a5	Prkd3	Nasp	
Mapkap1	Pcsk2	Scrn1	B3galt5	Pfn2	Npm3-ps1	Opalin	
E130309F12Rik	Scg5	Zfp523	Aplp1	Myo1b	Gna13	Nav1	
Dbp	Gm5868	Car12	Lyar	Tbp	Ctnnbip1	Pcyt2	
Itpka	Ctxn1	Ufsp1	Ttyh1	**Ppp2r5e**	Wnt7b	Parm1	
Pcsk2	Epor	Kars	Sipa1l3		Ptgis	Mical1	
Cbr3	Upb1	Socs5	Kdm3a		Srprb	Mobkl2a	

(*Tabel Continues*)

Table 1. Continued

Cluster D

UP 1–6 h			DOWN 1–6 h				
Nomo1	**Ppp1r1b**	Klf16	Gm10762	Cldn5	Ctsz	Igfbp2	Lix1
Dgat2	Tsen2	Mrps21	Dennd1c	Ctsc	Dlgap1	Gnas	Cotl1
Ttc17	Hnrnpl	Zfp281	Fam38b	Map3k1	Zeb2	Slc29a3	Fam81a
Ppp1r13b	Rundc3a	Ccbl1	Satb1	Stxbp1	Syn1	Vamp1	Myo9b
Oaz2-ps	Inpp5f	Plk2	Triobp	Cib2	Il18bp	Il4i1	Fadd
Fstl4	2010011I20Rik	Atxn1	Slc22a18	Fcgrt	Tcirg1	Chrna4	Tmem63b
Klf9	Rpap2	Ngef	Laptm5	Klhl6	Fes	Eif4g2	Tnr
Arl3	Scn4b	Tspan3	Mmp14	Cnih3	1700019N12Rik	Chchd8	Naglu
Bai2	**Hras1**	Agpat1	Cdkn1c	Pvalb	Gstm2	Chac1	2210012G02Rik
Sec14l1	Rpusd1	Sap130	Rab13	Tnfrsf19	Mitf	Axl	Cebpg
Gapdh	C2cd2l	Romo1	Rell1	Rassf5	Rapgefl1	Sh3pxd2b	Ncf4
Hbegf	Ppp1r1b	Amz2	Kcnc4	Bicc1	Ptprz1	Lasp1	Lamp2
Scube3	D2Wsu81e	Abcb8	2210411K11Rik	Sobp	Gabra3	Pqlc2	Vps13a
Cap1	Fam196b	Rbak	Ptplad2	Prickle1	Plek	Iqgap1	Robo2
Gpc3	Coro2b	Palm	Klhl6	Iqgap1	Lag3	Slamf9	9030612E09Rik
Ubqln4	Cox5b	Zfp704	Slc24a6	Hexa	Bbc3	Tirap	Aggf1
Sec14l1	Meis2	Siah2	Fxyd5	Mrpl48	Arhgap4	Palm2	Mak16
Taok1	Gm129	Darc	Col4a1	Arhgef19	P2ry6	Paox	Hcst
Mrpl33	Cry2	Gdf1	Cd200	Lat2	Pik3r1	Htatip2	Bach1
Trnp1	Cited4	Rc3h2	Slc44a2	Plcg2	Pik3cg	Myo9b	Pgm2l1
Thoc4	Sec14l1	St8sia3	**Mef2c**	Hecw1	Ftl1	Tab2	H2-K1
Tmem90a	Acy1		Clec2d	S1pr2	Stab1	Tgoln1	Grin1
			Arap1	Fbln1	Pik3r1	Pa2g4	Ppm1l
			Aif1	Trim25	Dpp7	Hvcn1	Crtac1
			Mef2c	Cyth4	Hspb6	Cask	Cd63
			Faah	Ctsz	Atp2a3	2410066E13Rik	2700060E02Rik
			Fadd	Mocs1	Sobp	Shc1	Rbl2
			Renbp	Gfap	2810416G20Rik	Serpinb6a	Daam1
			Chst8	Oasl2	Hapln4	Il11ra1	Gabrg2
			Ranbp3l	Npc2	Slc24a2	Ccnd1	Sepx1
			Igfbp5	Arrb2	Myl4	Efna5	Srpk3
			Lpp	Sox5	Syn2	Rsrc2	Fxyd5
			Sh3gl2	Fadd	Fcrls	St3gal5	Fbln2
			Rims1	Abi3	Snx9	Htatip2	C4b
			Cxcl12	Rbm6	Wdr1	Pdcd4	Oma1
			Ptprt	Nuak1	Lmna	Adar	
			Mapk11	Ganc	C4a	Capg	
			Tcirg1	Gstm2	Gatad2b	Il11ra1	
			Ltbp1	Uap1l1	Fgfr1op	C1qa	

The regulated mRNAs are identified by their official gene symbol. Each cluster is identified by the direction (UP: up-regulated, DOWN: down-regulated) and the peak of deregulation (1, 3, or 6 h after injection of L-DOPA). Genes are then sorted among the cluster by *p*-values. Genes in bold are those used for Figure 2.

MWG Operon, designed with Oligo Explorer 1.0, and verified for specificity with the NCBI Blast engine (www.ncbi.nlm.nih.gov/BLAST) using the "nearly exact short match" program. The forward and reverse oligonucleotides used for Nptx2, FosB, and Th were 5′-TTTGATGCCAC GCAGGCCTTTGT-3′ and 5′-TGGATCGTGGCCTCTGGGACG-3′, 5′-CCGTGAAACCGACAGAG-3′ and 5′-GAGTGGAATGAGATGCGAG-3′, 5′-AGGTCCGGGCCTTTGACCCA-3′ and 5′-AGCGCCGGATGGT GTGAGGA-3′ respectively. The end point PCR (35 cycles) was performed with LightCycler 480 SYBER Green I master (Roche) on 20 ng of RT product. After amplification, PCR products were analyzed by the melting curve to confirm the amplification specificity. The relative levels of mRNA were standardized using 36b4 ribosomal RNA as the nonvariant RNA. The quantitative RT-PCR on each sample was performed in triplicate. Expression values were determined using the ΔΔCT method.

Immunoblotting

Samples were homogenized in 1% SDS, equalized for their content in protein, and analyzed by Western blot. Homogenates were subject to SDS-PAGE on Bis-Tris gradient gels (4–12%; Invitrogen) with standard transfer and preblocking procedures. Membranes were incubated in a primary antibody overnight at 4°C. The antibody dilutions were 1:1000, 1:10000, 1:4000, 1:2000, 1:1000, and 1:1000 for primary antibodies corresponding to phospho-Thr202/Tyr204-ERK1/2 (Millipore), ERK1/2 (Sigma-Aldrich), TH (Sigma-Aldrich), Golf (Hervé et al., 1993), DARPP-32 (Gift from P.Greengard, Rockefeller University, New York, NY), and Narp (Tsui et al., 1996), respectively. Membranes were washed and incubated in a secondary antibody for 60 min at room temperature and then washed again. Secondary antibodies (1:4000) were IRDye 700DX-conjugated anti-rabbit IgG and IRDye 800CW-conjugated anti-mouse IgG (Rockland Immunochemical). Their binding was quantified using an Odyssey (LI-COR) infrared fluorescent detection system. Quantification was performed using Odyssey software (Odyssey infrared imaging system application, software version 1.2.15). The levels of phosphoproteins were normalized for the amount of the corresponding total protein detected in the sample.

Data analysis and statistics

Quality control of microarray was performed using Bead Studio (Illumina Genome Studio Software) and LumiR (www.bioconductor.org). Microarray data normalization on median and background was conducted using Bead Studio software (Illumina). Quality control before any array analysis included visualization of array scan images and observation of different quality markers of hybridization and homogeneity of expression, including, notably, the determination of signal/noise ratio, the average of detected genes, or the density of expression intensity. Microarrays for which >4 of the 16 observed indicators differed by >2 SDs from the mean were considered as bad quality control and were not

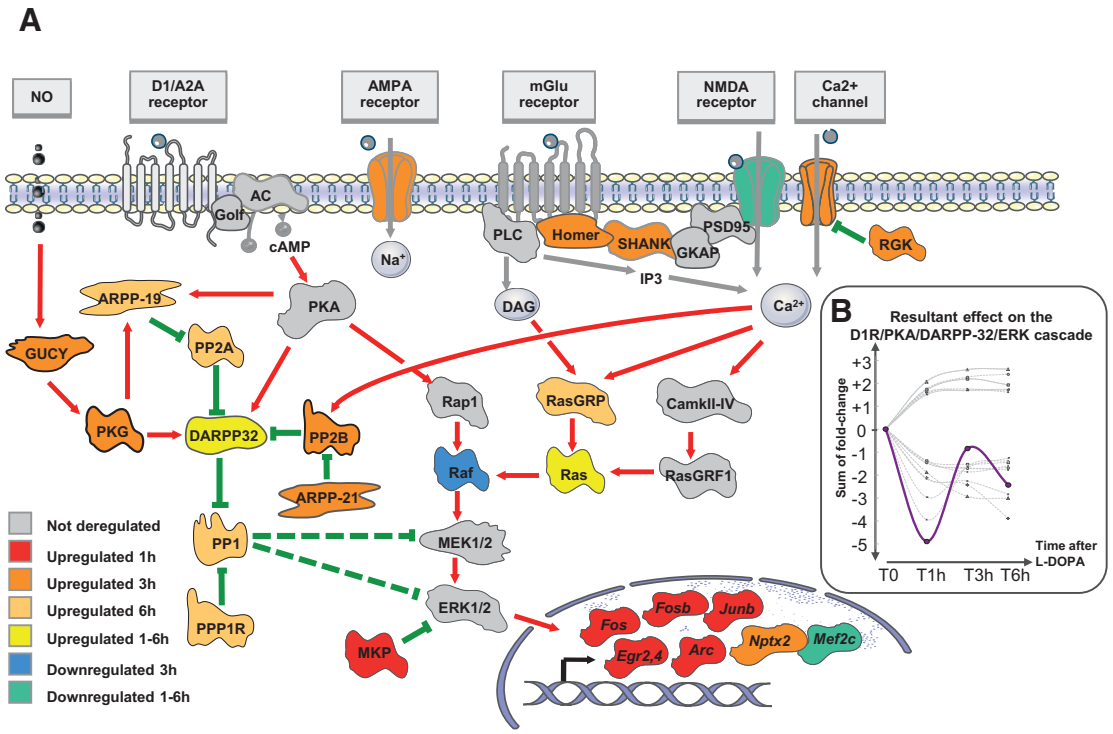

Figure 2. Model of the regulation of the D1R/PKA/DARPP-32/ERK cascade after an acute L-DOPA administration. ***A***, The proteins—or multiprotein complexes—of the D1R/PKA/DARPP-32/ERK are presented using different colors according to the time and the direction (up or down) of regulation of the corresponding gene(s) after the acute challenge of L-DOPA. Deregulated genes used for the figure are indicated in brackets: AMPA receptor: glutamate receptor ionotropic AMPA 2 (*Gria2*); NMDA receptor: glutamate receptor ionotropic NMDA 1 (*Grin1*) and Glutamate receptor ionotropic delta-2 (*Grid2*); Ca^{2+} channel: voltage-dependent calcium channel (*Cacna1h*, *Cacna2d3*, and *Cacnb2)*; Homer (*Homer1*); SHANK (*Shank3*); RGK (Rem2); ARPP-19; cAMP-regulated protein kinase of 19 kDa (*Arpp-19*); GUCY: guanylate cyclase (*Gucy1a3*); PKG: cGMP-dependent protein kinase (*Prkg2*); PP2A: protein phosphatase 2A (*Ppp2r2a*, *Ppp2r2c*, *Ppp2r2d*, *Ppp2r5e*); PP2B: protein phosphatase 2B (*Ppp3r1*); PP1: protein phosphatase 1 (*Ppp1cc*); PPP1R2: inhibitor-2 (*Ppp1r2*); MKP: MAP-kinase phosphatase (*Dusp1*, *Dusp6*); Raf (*Araf*); Ras (*Hras1*); RasGRP: RAS guanyl-releasing protein 1 (*Rasgrp1*). IEGs are also displayed (*Fos*, *FosB*, *Junb*, *Egr2*, *Egr4*, *Arc*, *Nptx2*, *Mef2c*). ***B***, Putative resultant effect on the D1R/PKA/DARPP-32/ERK cascade deregulation. A value corresponding to the fold change expression at each time point was attributed to each actor of the cascade with a positive (+1) or negative (−1) valence according to the expected effect on ERK activation. The purple curve corresponds to the overall resulting effect on ERK activation calculated as the arithmetic sum of each individual effect (gray curves). A negative value represents a putative downregulation of ERK activation; a positive value represents a putative upregulation of ERK activation.

included for further analyses. Over all of the experiments, 91% of microarrays passed the quality control. Microarray statistical analyses were performed using the Biometric Research Branch array tolls (http://linus.nci.nih.gov/BRB-ArrayTools.html) and the Multi Experiment Viewer software (MeV4.0; Saeed et al., 2003). General filters were applied before analysis and consisted of thresholding the minimal expression intensity at a value of 10 and in excluding probes if percentage missing exceeded 50%. Genes were identified as differentially expressed if they had a fold difference >1.2, if the univariate p-value was <0.01, and if the false discovery rate (FDR) was <0.1. For tests on a small number of genes, the FDR has not been applied but is shown in the tables anyway. Ontology analysis was assessed by using the functional annotation tool of the David Bioinformation database (http://david.abcc.ncifcrf.gov/; Huang da et al., 2009a, 2009b). A clustering image was obtained using average linkage clustering method with Multi Experiment Viewer software.

For blot quantifications, quantitative RT-PCR, and behavioral assessments, data are expressed as mean ± SEM. Comparisons between groups were performed using Mann–Whitney (for two groups) or Kruskal–Wallis ANOVA (for more than two groups). When two independent factors were analyzed (e.g., lesion and treatment or genotype and treatment), a 2-way ANOVA was used, followed by a Newman–Keuls *post hoc* test. An ANOVA for repeated measures was performed to analyze behavioral experiments. All analyses were performed using Statistica version 9.1 software (StatSoft).

Results

Acute L-DOPA signature

To identify the gene expression signature induced by an acute treatment with L-DOPA in the dopamine-denervated striatum, mice were treated with L-DOPA 20 mg/kg + benserazide 12 mg/kg intraperitoneally 4 weeks after unilateral injection of 6-OHDA into the striatum. The mice were killed 0, 1, 3, or 6 h after treatment to explore the time course of effects. Total mRNA was extracted from the dorsal striatum using a rapid freezing procedure to preserve RNA integrity (see Materials and Methods). Fifteen samples passed our quality control criteria and were retained for further analyses. After filtering, 11 029 probes were analyzed. We found 709 probes significantly deregulated at different time points, 376 were upregulated and 333 were downregulated (F test, univariate $p < 0.01$, FDR < 0.1; Fig. 1*A*, Table 1). The gene ontology analysis of this acute L-DOPA-induced gene expression signature showed significant enrichment in synapse-associated genes, synaptic transmission, and protein phosphatase activity (Fig. 1*B*). We identified four temporal profiles of gene expression by applying an unbiased self-organizing tree algorithm [self-organizing tree algorithm (SOTA), Multi Experiment Viewer software] on the 709 probes induced by L-DOPA (Fig. 1*C*, Table 1). Genes with a peak of expression 1 h after L-DOPA treatment belonged to "transcription regulator activity" and "MAPK signaling" pathways (Fig. 1*C*, cluster A). Not surprisingly, this cluster was composed of several immediate early genes (IEGs) known to be quickly induced by L-DOPA (*Fos*, *FosB*, *Junb*, *Egr2*, *Egr4*, *Nab2*, and *Arc*) in 6-OHDA-lesioned animals (Berke et al., 1998). The second cluster (cluster B) corresponded to genes with a maximal change of expression at 3 h either upregulated or downregulated. Genes in this cluster be-

longed to "long-term depression" and "gated channel activity" Gene Ontology pathways. The genes with a maximal deregulation at 6 h (cluster C) corresponded to genes with significant enrichment in the "protein phosphatase regulator activity." Finally, we found a cluster of long-lasting deregulated genes (1–6 h, cluster D), which was enriched in genes belonging to the "synaptic plasticity" and "synaptic transmission" pathways. Several genes deregulated by L-DOPA encoded proteins potentially involved in D1R/PKA/DARPP-32/ERK signaling pathways (Table 1). After a dramatic but transient increase of dual-phosphatases mRNA (*Dusp1* and *Dusp6*, peak of expression at 1 h), we observed a complex, long-lasting regulation of genes encoding protein phosphatase subunits. *Ppp1cc* (protein phosphatase 1, catalytic subunit, gamma isoform) and *Ppp1r2* (protein phosphatase 1 inhibitor 2) were upregulated with a maximal effect 6 h after L-DOPA. *Ppp3r1* (PP2B calcineurin B, type I) was upregulated with a more rapid peak of deregulation 3 h after L-DOPA. Finally, several subunits of PP2A were upregulated: *Ppp2r2a* (regulatory subunit B, PR 52, α isoform of PP2A), *Ppp2r2c* (regulatory subunit B, PR 52, gamma isoform of PP2A), and *Ppp2r5e* (regulatory subunit B, B56, ε isoform of PP2A) with a maximal upregulation 6 h after L-DOPA and *Ppp2r2d* (regulatory subunit B (PR55), delta isoform of PP2A) with a maximal upregulation 3 h after L-DOPA. Because these phosphatases may regulate the DIR/PKA/DARPP-32/ERK pathway in different ways, we wondered whether the molecular signature in response to L-DOPA would ultimately result in a positive or negative feedback upon the cascade. We represented deregulated genes in a model of the D1R/PKA/DARPP-32/ERK signaling pathways (Fig. 2*A*). To approximately model the overall effect of L-DOPA, we attributed to each molecular actor of the cascade a positive (+1) or negative (−1) valence according to its expected effect on ERK activation and a value corresponding to its fold-change expression after L-DOPA. The sum of the effects calculated at different time points suggested a rapid negative feedback on the D1R/PKA/DARPP-32/ERK cascade followed by an incomplete return to the basal state (Fig. 2*B*). This global negative feedback of the cascade would be an attractive explanation for the progressive decrease in ERK activation that has been observed after repeated administration of L-DOPA in nonhuman primates (Santini et al., 2010).

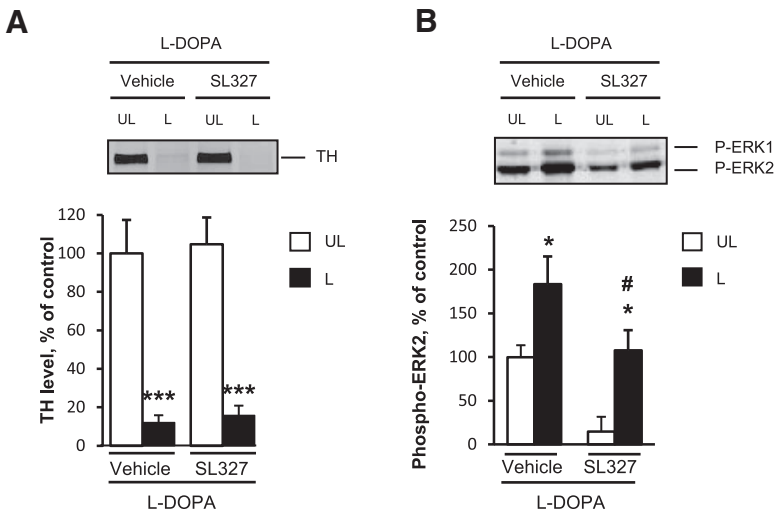

Figure 3. Striatal dopamine depletion induced by 6-OHDA and ERK inhibition by SL327 in L-DOPA treated mice. ***A***, Comparison of dopamine depletion in vehicle/L-DOPA-treated and SL327/L-DOPA-treated mice. Dopamine depletion in the striatum was assessed by determining the striatal levels of TH by immunoblotting in the 6-OHDA-lesioned (L) and unlesioned striata (UL) in mice treated with 20 mg/kg L-DOPA and pretreated with vehicle or 50 mg/kg SL327 ($n = 12$ per group). Data are expressed as means + SEM of percentage of the mean in the unlesioned striata (control). ***$p < 0.001$, lesioned versus unlesioned side, *post hoc* test. ***B***, Comparison of ERK phosphorylation in vehicle/L-DOPA-treated ($n = 4$) and SL327/L-DOPA-treated ($n = 4$) mice. Phospho-ERK1,2 in the 6-OHDA-lesioned (L) and unlesioned striata (UL) was assessed by immunoblotting 30 min post-L-DOPA treatment. Data correspond to percentage of the mean in the unlesioned-vehicle samples and are expressed as means + SEM. *$p < 0.05$, L versus UL, #$p < 0.05$, SL327 versus vehicle, *post hoc* test.

ERK-dependent genes

Because the inhibition of ERK activation was previously demonstrated to decrease L-DOPA-induced AIMs in lesioned mice (Santini et al., 2007; Fasano et al., 2010), we decided to identify genes regulated by ERK activity among those in the above L-DOPA-induced signature. To block ERK activation, the MEK inhibitor SL327 (50 mg/kg) or vehicle was administered intraperitoneally 30 min before L-DOPA in a new experiment. Some mice were killed 3 h after L-DOPA, the time for which we found the highest number of deregulated genes, and another group of mice were killed 30 min after L-DOPA to study the effect of SL327 on ERK phosphorylation. By immunoblot, we confirmed that the level of dopamine depletion as evaluated by tyrosine hydroxylase levels was similar between the groups (vehicle or SL327-treated mice: 2-way ANOVA, lesion effect: $F_{(1,46)} = 59.3$, $p < 0.001$; SL327 effect: $F_{(1,46)} = 0.14$, not significant (ns); lesion and SL327 interaction: $F_{(1,46)} = 0.002$, ns; Figure 3*A*) and that ERK phosphorylation was increased in the 6-OHDA-lesioned side compared with the unlesioned side and decreased in the striatum of SL327-treated animals (2-way ANOVA, lesion effect: $F_{(1,12)} = 15.4$, $p < 0.01$; SL327 effect: $F_{(1,12)} = 12.8$, $p < 0.01$, SL327 effect; interaction: $F_{(1,12)} = 0.8$, ns; Figure 3*B*). To selectively identify the genes for which deregulation by L-DOPA was blocked by the SL327, we restricted the analysis to the 709 probes deregulated by L-DOPA and identified those with expression that varied in the opposite direction (e.g., upregulated with L-DOPA compared with vehicle, and downregulated when mice were treated with L-DOPA + SL327 compared with L-DOPA + vehicle). We found 28 genes significantly blocked by SL327 by using this strategy (Table 2). When genes were ranked by fold change (Table 2), *FosB* was at the top of the list of genes, in agreement with previous reports showing that the induction of *FosB* was associated with ERK activation in 6-OHDA-lesioned mice (Pavón et al., 2006).

Genes associated with AIMs

Our final goal was to identify genes involved in the early development of LID. Gene expression differs dramatically after one or repeated administrations of L-DOPA (Cenci and Konradi, 2010) and AIMs progressively increase in intensity after repeated administration of L-DOPA (Lundblad et al., 2005; Putterman et al., 2007; Nadjar et al., 2009; Francardo et al., 2011). The final score of AIMs obtained in mice injected with 6-OHDA in the striatum is usually variable, leading to the ability to distinguish highly and weakly dyskinetic animals (Lundblad et al., 2004) referred to below as high dyskinetic (HD) and low dyskinetic (LD). To study early gene expression changes associated with the development of

Table 2. List of genes deregulated by L-DOPA and blocked by SL-327

Official gene symbol	Nucleotide universal identifier	L-DOPA vs saline (fold change)	L-DOPA + SL327 vs L-DOPA + vehicle (fold change)	Univariate *p*-value*	FDR*
FosB	Ere3vD3o.tqh0Q.x94	+8.76	−2.08	0.0075	0.021
Arc	oyruyspXqhyohXojdA	+4.49	−1.56	0.0196	0.036
Nptx2	BU2LP1VoHoj2ptP6ec	+4.09	−1.87	0.0066	0.020
Ccrn4l	ruOG_shu4l8dQ0fdeo	+3.95	−1.22	0.0102	0.026
Dgki	ZnFK.QqcSo7EEoRjJU	+3.69	−1.22	0.0325	0.048
Nedd4l	ESdC5ZVdFlD3Qevluw	+3.21	−1.34	0.0003	0.003
Car12	re1dJUylHuMPt50k.U	+2.84	−1.25	0.0020	0.010
C8b	HERl41YuB1BXREfJSk	+2.62	−1.53	0.0239	0.041
Zfp280d	uLS7MJ7kgVRdJVTgcs	+2.48	−1.26	0.0406	0.058
Ippk	idcnpHiD3Gq0Ugu5ek	+2.43	−1.37	5.29E-05	0.002
Th	Ko4nkRXhUJHi5TycDk	+2.32	−1.40	0.0290	0.046
Dmkn	3akQXpeeC6eC0.6yBPU	+2.20	−1.36	0.0049	0.018
Dmkn	Nmh10YORErfSov4e18	+2.03	−1.33	0.0040	0.016
Kcnk1	6VF0RwJEOktVd1XgSM	+1.66	−1.20	0.0002	0.003
Agpat1	NI5Q.efVXJdFXlUrLo	+1.62	−1.23	0.0315	0.048
Mocs1	creVEXtx3pO7SgCibQ	−2.72	+1.22	0.0007	0.005
Mef2c	9r_hIVpC64cWsPsoEY	−2.49	+1.28	0.0040	0.016
Gm10762	KlFvB5mECAoFSh6a0.0	−2.47	+1.49	0.0157	0.032
Pa2g4	EpeAOAH0bl0.9LiugaY	−2.33	+1.21	0.0245	0.041
Bbc3	uioaVJewjHsTkeeyMw	−2.30	+1.36	0.0155	0.032
Ganc	3qeocgyRKj6R_3ykYU	−2.26	+1.26	0.0003	0.003
Hecw1	3TeO9EhFExAnkiRjrk	−2.17	+1.63	0.0013	0.008
Arrb2	fladaeCoOCjjh7jhS8	−2.12	+1.23	0.0016	0.009
Cln6	Ed_ISRN0l4N3RReXrk	−2.07	+1.32	0.0188	0.036
Syt12	TrSLz4qjZNMbiuentE	−1.92	+1.22	0.0057	0.019
Tusc1	HpdSI3.yLN94SuOP4k	−1.76	+1.27	0.0122	0.029
Vstm2a	3.EkJQO7FbNLDvRTn4	−1.58	+1.22	0.0102	0.026
3632451006Rik	oPE5K3u7N_TwP9SXfs	−1.38	+1.22	0.0160	0.032

List of the 28 probes deregulated by L-DOPA (our first experiment, 709 probes) for which SL327 pretreatment significantly reduced the effects of L-DOPA (that could be increase or decrease) (>1.2-fold, $p < 0.05$, FDR < 0.1). The fold changes of expression induced 3 h after L-DOPA in the first experiment (compared with T0, left column) and 3 h after L-DOPA + SL327 (compared with L-DOPA + vehicle, right column) are presented.

*p-values and FDR values for the comparison of gene expression between L-DOPA + SL327 and L-DOPA + vehicle.

a HD score, we investigated whether it would be possible to predict at the very beginning of the treatment which mice will later develop high scores of AIMs. We treated 6-OHDA-lesioned mice with a daily injection of L-DOPA for 9 d and observed a strong correlation of AIM scores between days 2 and 9 ($r^2 = 0.84$, $p < 0.0001$; Fig. 4*A*). We therefore considered the AIM score after the second administration of L-DOPA as a good predictor of future LID development. Other groups of mice were then treated with 2 injections of L-DOPA (20 mg/kg, $n = 18$) or vehicle ($n = 7$) separated by a 24 h interval. At day 2, AIMs were assessed during 2 h after L-DOPA treatment and mice were killed 1 h later. The mice treated with L-DOPA were then segregated according to their AIM score to compare the two extreme quartiles (HD mice, $n = 4$; LD mice, $n = 5$). The score of AIMs (ALO score) in the LD group was 8.6 ± 5.9 vs 36.3 ± 8.7 in the HD group ($p < 0.05$; Fig. 4*B*). The differences observed in AIM score were unlikely to be due to differences related to the lesion's extent because the limb use asymmetry measured by the cylinder test, the L-DOPA-induced rotation, and the quantification of TH immunoblots in the striatum were similar between the HD and LD groups (Fig. 4*B*). We compared the expression of the 709 probes previously found to be deregulated by L-DOPA (our first experiment) between the LD and HD mice. We found 26 genes that were significantly different between these two groups (Fig. 4*C*, Table 3). As for the previous experiments, *FosB* was found in the top gene list: *FosB* expression was significantly higher in the striatum of HD than in LD mice, which is consistent with several previous reports (Pavón et al., 2006; Cao et al., 2010).

Genes deregulated by L-DOPA, dependent on ERK activation, and associated with AIMs

Finally, we considered genes induced by the first administration of L-DOPA (first experiment), blocked by SL327 pretreatment (second experiment), and differentially expressed between the HD and LD mice (third experiment) as those of particular interest. This intersect list was composed of five genes (Table 4): *Nptx2*, *Nedd4l*, *FosB*, *Th*, and *Ccrn4l*. Interestingly *FosB*, *Th*, and *Nptx2* have all been previously reported to be induced by stimulation of D1R in 6-OHDA-lesioned animals (Berke et al., 1998, Darmopil et al., 2008). *FosB* was already shown to be involved in LID (Andersson et al., 1999). In our experiments, *FosB* expression was increased 12-fold after the first administration of L-DOPA (1 h; Table 1); its expression was decreased by >2-fold when SL327 was administrated before L-DOPA (Table 2); and its expression was 2-fold higher in HD mice compared with LD animals as soon as the second administration of L-DOPA (Table 3). We confirmed by quantitative RT-PCR the increase in *FosB* expression in the lesioned striatum after L-DOPA, its decrease after pretreatment with SL327 (2-way ANOVA, lesion effect: $F_{(1,36)} = 39.0$, $p < 0.001$; SL327 effect $F_{(1,36)} = 12.0$, $p < 0.01$; interaction: $F_{(1,36)} = 9.8$, $p < 0.01$; Fig. 5*A*) and its higher expression level in HD animals (Kruskal–Wallis ANOVA, $H_{(2,13)} = 10.7$, $p < 0.01$; Fig. 5*B*). *Th* encodes TH, the enzyme transforming tyrosine into the precursor of dopamine, L-DOPA. In normal conditions, TH is quasi-exclusively expressed in brainstem noradrenergic and dopaminergic neurons. However, TH-immunoreactive neurons have been detected in the striatum after dopamine depletion in animals and parkinsonian patients (Huot

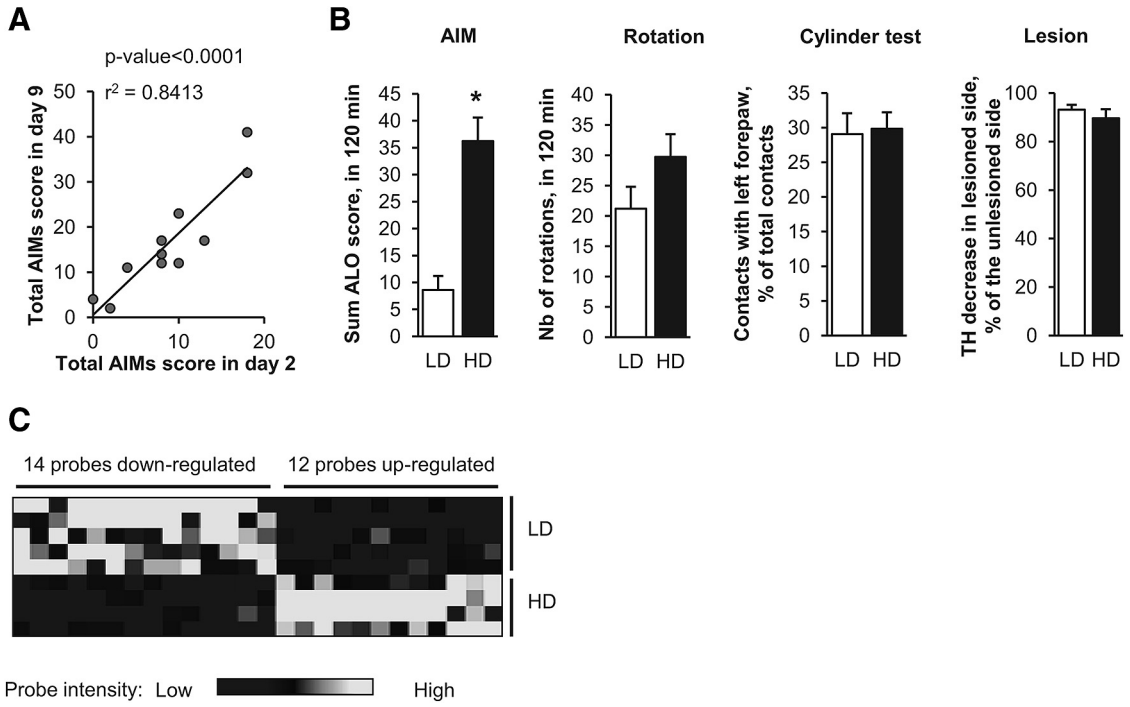

Figure 4. Gene expression signature associated with L-DOPA-induced dyskinesia. ***A***, Correlation between AIM scores on days 2 and 9 of L-DOPA administration in the same mice. The second injection of L-DOPA is highly predictive of the ability to develop AIMs, as evidenced by the high correlation between the total AIM score on days 2 and 9 of L-DOPA administration (Spearman $r^2 = 0.84$, $p < 0.0001$) performed on 11 lesioned mice. ***B***, Behavioral scores and quantifications of TH level reductions in HD and LD. Eighteen 6-OHDA-lesioned mice were tested for the limb use asymmetry by the cylinder test, treated with L-DOPA for 2 consecutive days, and scored for ALO dyskinesia and rotation for 2 h after a second L-DOPA injection. LD ($n = 5$) and HD ($n = 4$) mice were separated according to ALO scores (lowest and highest quartiles) and compared for the various parameters. Data are expressed as means + SEM. *$p < 0.05$, HD versus LD. The number of L-DOPA-induced rotations, the limb use asymmetry measured by the cylinder test, and the dopaminergic denervation were not statistically different between the two groups, contrasting with their significant difference in L-DOPA-induced dyskinesia. ***C***, Heat map of the 26 significantly deregulated probes (fold change > 1.2, $p < 0.05$) between HD and LD mice among the 709 probes found deregulated by an acute challenge of L-DOPA (Fig. 1). Hierarchical clustering of genes and samples was performed using one minus correlation metrics and average linkages with Biometric Research Branch array tools. The black probes correspond to downregulated genes and white probes correspond to upregulated genes.

et al., 2007). In our experiments, *Th* expression increased by >3-fold after L-DOPA (6 h; Table 1), decreased by 1.4-fold after SL327 (Table 2), and was 2-fold higher in HD than in LD animals (Table 3). These various effects on *Th* expression were confirmed by quantitative RT-PCR (2-way ANOVA, lesion effect: $F_{(1,31)} = 2.0$, ns; SL327 effect: $F_{(1,31)} = 8.6$, $p < 0.01$, interaction: $F_{(1,31)} = 7.2$, $p < 0.05$; Fig. 5*C*; Kruskal–Wallis ANOVA, $H_{(2,13)} = 9.2$, $p < 0.01$; Fig. 5*D*).

We next focused on *Nptx2* because it was the most statistically significant gene between HD and LD animals ($p = 0.0014$; Table 4). *Nptx2* expression was increased by 4-fold after acute treatment with L-DOPA, with a maximal upregulation at 3 h (Kruskal–Wallis ANOVA, $H_{(3,15)} = 9.0$, $p < 0.05$; Fig. 6*A*). This upregulation was repressed by SL327 pretreatment (2-way ANOVA, lesion effect: $F_{(1,39)} = 34.8$, $p < 0.001$; SL327 effect: $F_{(1,39)} = 8.0$, $p < 0.01$; interaction: $F_{(1,39)} = 2.2$, $p < 0.05$; Fig. 6*B*) and *Nptx2* expression was 2-fold higher in HD than in LD mice (Fig. 6*C*). Quantitative RT-PCR confirmed its increased expression by 4-fold 3 h after L-DOPA in the dopamine-denervated striatum (mean relative expression values ± SEM: T0 (100 ± 7), T1h (127 ± 3), T3h (383 ± 34), T6h (152 ± 15), Kruskal–Wallis ANOVA, $H_{(3,16)} = 12.5$, $p < 0.01$, posttest $p = 0.003$ at 3 h, data not shown). L-DOPA-induced *Nptx2* expression was significantly reduced by SL327 pretreatment (2-way ANOVA, lesion effect: $F_{(1,36)} = 8.5$, $p < 0.001$; SL327 effect: $F_{(1,36)} = 5.4$, $p < 0.05$; interaction: $F_{(1,36)} = 2.2$, ns; Fig. 6*B*) and 2-fold higher in HD than in LD mice (Kruskal–Wallis ANOVA, $H_{(2,16)} = 12.1$, $p < 0.01$; Fig. 6*C*).

L-DOPA-induced dyskinesia are decreased in Narp KO mice

Nptx2 is an IEG induced by D1R stimulation in the striatum of 6-OHDA-lesioned rats (Berke et al., 1998) and encodes a neuronal activity-regulated pentraxin, Narp (also known as neuronal pentraxin II; Tsui et al., 1996). We investigated the possible role of Narp in LID by examining AIM development in mutant mice in which the *Nptx2* gene had been invalidated (Narp KO mice; Bjartmar et al., 2006). Narp KO mice have neither apparent neurological deficit nor brain dysfunction (Bjartmar et al., 2006). Spontaneous locomotor activity of Narp KO mice was reported previously to be similar to WT mice (Pacchioni and Kalivas, 2009). To confirm these results, NARP KO mice ($n = 6$) and WT littermates ($n = 8$) were placed in a circular corridor where spontaneous locomotor activity was assessed for 90 min. The locomotor activity was not significantly different between genotypes (1/4 turns during 90 min (mean ± SEM): Narp KO 255 ± 36, WT mice 261 ± 53, Mann–Whitney test, ns). We first examined whether striatal proteins important for the signaling responses involved in LID generation were altered in Narp KO mice. Immunoblotting did not reveal any significant change in the striatal levels of Gαolf, the G-protein subunit coupling D1R to adenylyl cyclase in the striatum, the regulatory protein DARPP-32, or ERK 1 and ERK2 in the mice with homozygous or heterozygous deletion of Narp gene (Kruskall-Wallis ANOVA, ns for Gαolf, ERK1, ERK2, DARPP-32, and actin; $H_{(2,35)} = 9.8$, $p < 0.05$, for Narp; Fig. 7*A*). This suggested no gross alteration of the D1R-dependent signaling cascade proteins in Narp KO mice. To investigate the role of Narp in LID development, Narp KO mice and

Table 3. LID signature: deregulated genes between high and low dyskinetic animals

Official gene symbol	Nucleotide universal identifier	Univariate *p* value	FDR	HD/LD (fold change)	Probe intensity	
					LD	HD
FosB	Ere3vD3o.tqh0Q.x94	0.0052	0.06	+2.09	905	1891
Nptx2	BU2LP1VoHoj2ptP6ec	0.0014	0.05	+1.91	1016	1936
Th	Ko4nkRXhUJHi5TycDk	0.0111	0.11	+1.77	86	152
Tirap	6kxeKn6PcXUkUUAQKI	0.0373	0.16	+1.43	23	34
Tac1	HZWCFQI0kvf6PDqQmo	0.0129	0.11	+1.41	4634	6516
Car12	f2X7nXwd5bmK5Curlw	0.0103	0.11	+1.33	384	511
Arg2	rHekX9EEk8SL5Ck9go	0.0173	0.11	+1.33	181	241
Ccrn4l	ruOG_shu4I8dQ0fdeo	0.0458	0.17	+1.25	1524	1907
Ece1	6PnSruSolCkolZlevl	0.0304	0.15	+1.23	483	593
Zfp281	rsQiwIRUUIlvErCt2l	0.0014	0.05	+1.21	252	305
Nedd4l	ESdC5ZVdFID3Qevluw	0.0051	0.06	+1.21	1257	1518
Lingo3	HVVh.VNExAePhKEYOE	0.0480	0.17	+1.20	171	205
Tmem106c	fVTEC48S.VWQq3Ngqc	0.0363	0.16	−1.20	276	230
Triobp	6hH3fe9bi0VwfDAF9Y	0.0022	0.05	−1.21	241	199
Nol3	KIzuSJ1_7O3uHryFUY	0.0164	0.11	−1.22	162	133
Paox	ovot6freNOjlW8LvsY	0.0162	0.11	−1.24	112	90
Slc2a6	KUtQF_jF3LeUHvR7.0	0.0031	0.06	−1.25	170	137
Fadd	9Snh4rufElernL7g6l	0.0188	0.11	−1.26	33	26
Nuak1	9XrnfxQKJ2eSrgPSm4	0.0051	0.06	−1.27	628	495
Arhgap4	Bpc_fRdJXfcrd_orJA	0.0171	0.11	−1.28	35	27
Igfbp5	ZVY7oInadd.JP_sfCg	0.0474	0.17	−1.35	1025	757
Rell1	97rI5L_O4FRHpJy4fo	0.0459	0.17	−1.36	39	29
F11r	QdMHGeZ9IbdAfQUHac	0.0332	0.15	−1.37	30	22
Mapk11	ipXv4AZvqrsGXV4lhA	0.0151	0.11	−1.37	64	46
Fam113a	ol6MpKN8r6JylxS6V4	0.0267	0.14	−1.38	64	47
Metap1d	iqi6Ix4UB5RCCXiDaU	0.0204	0.11	−1.40	41	30

List of the 26 genes significantly different between HD and LD animals among the 709 genes found to be deregulated by acute L-DOPA in the striatum (our first experiment).

Table 4. Genes deregulated by L-DOPA associated with LID and dependent on ERK

Official gene symbol	Nucleotide universal identifier	Probe intensity		HD vs LD (fold change)	Univariate *p*-value
		LD	HD		
Nptx2	BU2LP1VoHoj2ptP6ec	1016	1936	+1.9	0.0014
Nedd4l	ESdC5ZVdFID3Qevluw	1257	1518	+1.2	0.0051
FosB	Ere3vD3o.tqh0Q.x94	905	1891	+2.1	0.0052
Th	Ko4nkRXhUJHi5TycDk	86	152	+1.8	0.0111
Ccrn4l	ruOG_shu4I8dQ0fdeo	1524	1907	+1.3	0.0458

List of the five genes belonging to the acute L-DOPA signature (Table 1), the genes blocked by SL327 (Table 3), and the genes associated with dyskinesia (this table). Probe intensity in microarrays, fold change, and univariate *p*-values are provided comparing HD versus LD animals.

WT littermates were unilaterally injected with 6-OHDA into the striatum and chronically treated with L-DOPA using an escalating dose protocol (5, 10, and 20 mg/kg i.p. daily for 5 d for each dose; Lundblad et al., 2004). The reduction in TH immunoreactivity in the striatum was similar in WT and Narp KO mice, showing that the lesion of dopamine neurons was comparable in the two groups of mice (2-way ANOVA, lesion effect: $F_{(1,66)} = 65.34$, $p < 0.001$; genotype effect: $F_{(1,66)} = 0.85$, ns; interaction, $F_{(1,66)} = 0.09$, ns; Fig. 7*B*). We then compared AIMs in mutant and WT mice. We observed a significant decrease in AIM score in Narp KO mice compared with WT mice throughout the escalating doses (2-way repeated-measures ANOVA, genotype effect: $F_{(1,36)} = 4.13$, $p < 0.05$; dose effect: $F_{(2,72)} = 49.84$, $p < 0.001$; interaction: $F_{(2,72)} = 1.39$, ns; Fig. 7*C*). *Post hoc* analysis found a significantly decreased score in the mutant mice at the end of the trial at 20 mg/kg L-DOPA (Newman–Keuls, $p < 0.05$; Fig. 7*C*). At this dose, the time course of L-DOPA effects on AIMs indicated that the reduction was present throughout the period of action of L-DOPA (2-way repeated-measures ANOVA, genotype effect: $F_{(1,36)} = 6.17$, $p < 0.05$; time effect: $F_{(5,180)} = 19.23$, $p < 0.001$; interaction: $F_{(5,180)} = 2.32$, $p < 0.05$; Fig. 7*D*). These results indicated that Narp is implicated in the development of AIMs induced by L-DOPA in unilaterally 6-OHDA lesioned mice.

Nptx2 in the striatum is involved in the development of L-DOPA-induced dyskinesia

To investigate whether Narp secretion in the striatum is involved in the development of LID, we used a mutant form of Narp that blocks secretion of WT Narp (Narp-N13) and a mutant that does not block secretion of WT Narp (Narp-N; O'Brien et al., 2002). In HEK293 cells, Narp-N13 prevented its secretion and reduced secretion of coexpressed WT Narp (Fig. 8*A*). Narp-N13 prevented expression of WT Narp on the cell surface of HEK293 cells (Fig. 8*B*). Narp-N did not prevent secretion of coexpressed WT Narp (Fig. 8*A*). WT mice were then injected in the dorsal striatum, concomitantly to 6-OHDA, with a recombinant AAV expressing Narp-N13 (AAV-DN13), Narp-N (AAV-Narp-N), or the green fluorescent protein (AAV-eGFP). Mice were chronically treated with L-DOPA using the same escalating dose protocol as for Narp KO mice. The reduction in TH immunoreactivity in the striatum was similar in all groups of mice (2-way ANOVA, lesion effect: $F_{(1,18)} = 60.7$, $p < 0.001$; group effect: $F_{(2,18)} = 0.5$, ns; interaction: $F_{(2,18)} = 0.17$, ns; Fig. 8*C*). Mice injected with AAV-DN13 had a dramatic decrease of AIMs score compared with those injected with AAV-eGFP (2-way ANOVA, AAV effect: $F_{(1,12)} = 8.2$, $p < 0.01$; dose effect: $F_{(2,24)} = 18.7$, $p < 0.001$; interaction: $F_{(2,24)} = 8.4$, $p < 0.01$) or AAV-Narp-N (2-way ANOVA, AAV effect: $F_{(1,12)} = 5.9$, $p < 0.05$; dose effect: $F_{(2,24)} = 6.7$, $p < 0.01$; interaction: $F_{(2,24)} = 2.2$, ns; Fig. 8*D*). At 20 mg/kg, AIM scores were significantly different for AAV-DN13 compared with AAV-eGFP (2-way repeated-measures ANOVA, AAV effect: $F_{(1,12)} = 4.5$, $p < 0.05$; time effect: $F_{(4,48)} = 4.5$, $p < 0.05$; interaction: $F_{(4,48)} = 3.8$, $p < 0.01$) or to AAV-Narp-N (2-way repeated-measures ANOVA, $F_{(1,12)} = 4.9$, $p < 0.05$; time effect: $F_{(4,48)} = 1.8$, ns; interaction: $F_{(4,48)} = 1.5$, ns; Fig. 8*E*). Mice injected with the AAV-Narp-N were not significantly

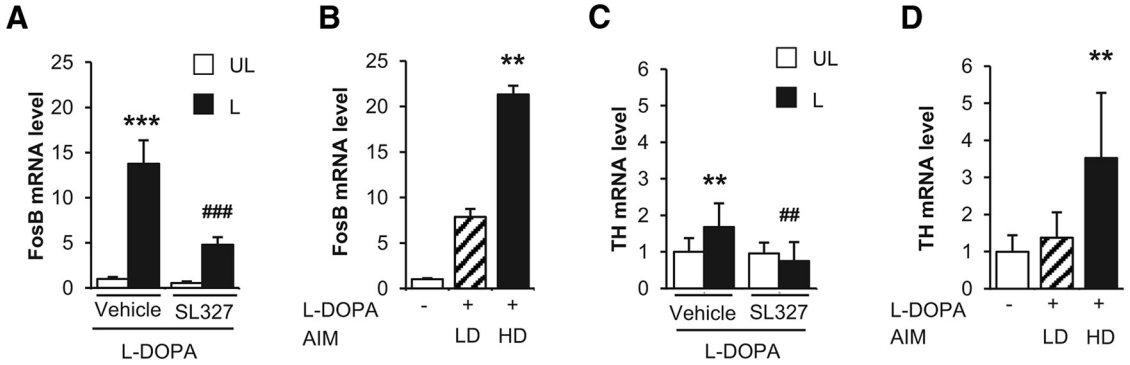

Figure 5. Quantitative RT-PCR indicates high expression of *FosB* and *Th* genes in dyskinetic animals. Relative expression of FosB (***A***, ***B***), and TH (***C***, ***D***) assessed by independent quantitative RT-PCR from striata of 6-OHDA-lesioned mice. In a first experiment (***A***, ***C***), total mRNA was extracted from the lesioned (L) and the unlesioned (UL) striatum of mice treated with 20 mg/kg L-DOPA and pretreated with 50 mg/kg SL327 or vehicle 30 min before L-DOPA ($n = 8–9$ per group). Mice were killed 3 h after L-DOPA treatment. In a second experiment (***B***, ***D***), total mRNA was extracted from the 6-OHDA-lesioned striatum of LD ($n = 5$) and HD ($n = 4$) mice (as defined in the Materials and Methods), as well as saline-treated animals (white boxes, $n = 5$). Each reverse transcription was performed in triplicate. The relative levels of mRNA were standardized using 36b4 ribosomal RNA as the nonvariant RNA. Expression values were determined using the ΔΔCT method. Data are expressed as mean fold change + SEM compared with the means in vehicle-L-DOPA unlesioned striata (***A***, ***C***) or saline lesioned striata (***B***, ***D***). *Post hoc* tests: ***A***: ***$p < 0.001$, lesioned versus unlesioned side, ###$p < 0.001$, SL327 versus vehicle; ***B***, **$p < 0.01$ HD versus saline; ***C***: **$p < 0.01$, lesioned versus unlesioned side, ##$p < 0.01$, SL327 versus vehicle; ***D***: $p < 0.01$, **$p < 0.01$ versus saline.

different from those injected with AAV-eGFP. Together, these results demonstrate that Narp secretion in the striatum is necessary for the LID development.

Discussion

Using an unbiased transcriptomic approach taking into account the time course of the effects, we identified a detailed gene expression signature induced by the first injection of L-DOPA in the striatum of unilaterally 6-OHDA-lesioned mice. We subsequently restricted this signature to genes in which deregulation was prevented by a MEK inhibitor, SL327. Finally, among those genes, we identified five that were associated with early LID development, *FosB*, *Th*, *Nptx2*, *Ccrn4l*, and *Nedd4l*. We focused on *Nptx2*, which encodes Narp, a protein regulating synaptic plasticity (Xu et al., 2003). We show that *Nptx2* is an important factor in LID development by demonstrating that AIMs induced by a chronic treatment with L-DOPA in 6-OHDA-lesioned mice are decreased in Narp KO mice or by striatal expression of a dominant-negative mutant of Narp.

Gene expression analysis in the dopamine-depleted striatum highlighted a complex transcriptional response to acute L-DOPA administration. Our gene ontology analysis supports previous suggestions that L-DOPA changes corticostriatal synaptic plasticity homeostasis (Calabresi et al., 2000; Calon et al., 2000; Picconi et al., 2003), which results from the successive regulation of IEGs followed by a longer-lasting gene expression response (El Atifi-Borel et al., 2009; Cenci and Konradi, 2010). We found that L-DOPA regulates multiple catalytic and regulatory components of the D1R/PKA/DARPP-32/ERK cascades, which are thought to be implicated in LID development (Santini et al., 2007; Bateup et al., 2010). Overall, our results suggest that L-DOPA-induced gene expression in the striatum results in a rapid and profound downregulation of these cascades followed by a slow progressive return to basal level. This regulation is in agreement with the progressive decrease in L-DOPA-induced ERK phosphorylation and IEG production in the dopamine-denervated striatum after prolonged chronic treatment (Santini et al., 2007; Cenci and Konradi, 2010; Ding et al., 2011). Alterations of protein phosphatases at the mRNA level have been previously reported after dopamine depletion in rats by Meurers et al. (2009) who proposed that dopaminergic denervation resulted in "prodopaminergic phosphorylation" patterns. Our present results suggest that L-DOPA counteracts this state by producing a strong negative feedback on dopamine signaling. Together, these data indicate that dopamine regulates PKA/DARPP-32/ERK cascades through changes in protein phosphatase expression, resulting in their sensitization after dopamine depletion and their downregulation after treatment with L-DOPA. The mechanisms by which dopamine regulates the expression of protein phosphatases remain to be explored. None of these genes was significantly blocked by SL327 pretreatment in our experiments, suggesting an ERK-independent pathway.

D1R/PKA-mediated activation of ERK signaling after dopamine depletion has been suggested to play a major role in AIM development (Gerfen et al., 2002; Picconi et al., 2003; Santini et al., 2007; Westin et al., 2007; Schuster et al., 2008; Darmopil et al., 2009; Lindgren et al., 2009; Santini et al., 2009a; Santini et al., 2009b; Lebel et al., 2010; Santini et al., 2010; Francardo et al., 2011). The role of DARPP-32 in ERK activation by L-DOPA is debated because ERK phosphorylation was decreased in DARPP-32 KO mice in one study (Santini et al., 2007), but not in another one (Gerfen et al., 2008). A recent report using conditional KO of DARPP-32 in D1 MSN or a knock in mutation preventing phosphorylation of DARPP-32 by PKA support the role of DARPP-32 (Santini et al., 2012) and that LID is attenuated either by DARPP-32 general or conditional mutation (Santini et al., 2007, 2012, Bateup et al., 2010) or by blockade of ERK activation (Santini et al., 2007, Fasano et al., 2010). LID is proposed to result from a maladaptive plasticity of striatal neurons and long-term cellular alterations produced by the intense activation of ERK-dependent signaling pathways after the first L-DOPA treatments (Cenci and Konradi, 2010), whereas ERK activation ends to decrease in MSNs with repeated drug administration (Santini et al., 2007; Ding et al., 2011). In rats, only a few of the genes regulated after acute L-DOPA administration overlapped with those expressed after chronic exposure (El Atifi-Borel et al., 2009). By focusing on genes induced by the first administrations of L-DOPA, blocked by the MEK inhibitor SL327, and associated with the early development of AIMs, we postulated that we would be able to identify candidates involved in LID induction. Among the 5 genes identified by this approach, *FosB* was previously shown to be induced by L-DOPA and associated with dyskinesia

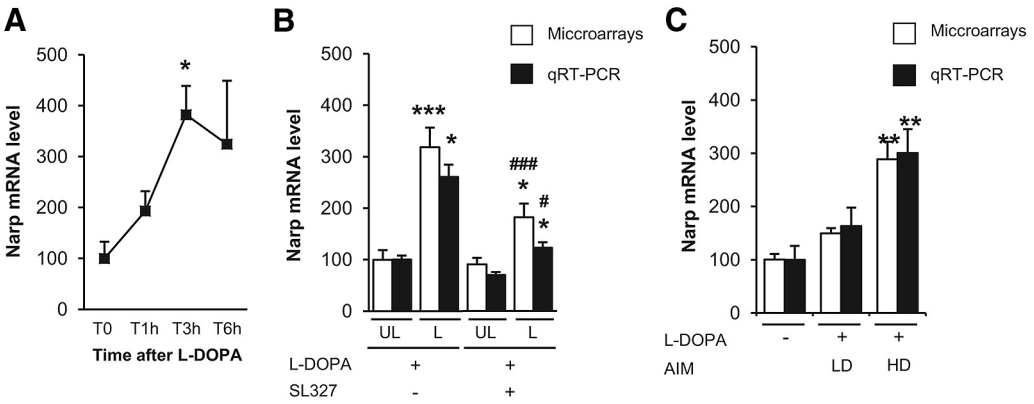

Figure 6. Increased expression of *Nptx2* in dyskinetic mice. ***A***, Time course of *Nptx2* deregulation as assessed by expression values in microarray experiments 1, 3, and 6 h after an acute administration of 20 mg/kg L-DOPA in the 6-OHDA-lesioned striatum. Data correspond to percentage of the mean of T0 samples and are expressed as mean + SEM (T0, $n = 3$; T1h, $n = 4$; T3h, $n = 5$; T6h, $n = 3$). *Nptx2* was significantly induced by L-DOPA. *$p < 0.05$, *post hoc* test. ***B***, Effect of the MEK inhibitor (SL327) on the expression of *Nptx2* in microarray experiments (white boxes) and quantitative RT-PCR (black boxes). Total mRNA was extracted from the lesioned (L) and the unlesioned (UL) striatum 3 h after treatment with 20 mg/kg L-DOPA and pretreatment with 50 mg/kg SL327 or vehicle 30 min before L-DOPA ($n = 10–11$ per group). Data were normalized on unlesioned group treated with vehicle. Data are expressed as mean + SEM. ***$p < 0.001$, *$p < 0.05$, lesioned versus unlesioned, ###$p < 0.001$, #$p < 0.05$, SL327 versus Vehicle, *post hoc* test. ***C***, *Nptx2* expression in LD and HD mice after 2 injections of L-DOPA in 6-OHDA lesioned mice. Microarrays (white boxes) and quantitative RT-PCR (black boxes) expression values were obtained as detailed above from total mRNA extracted from the 6-OHDA-lesioned striatum of LD ($n = 5$), HD ($n = 4$), and saline-treated mice ($n = 7$). Data were normalized on saline-treated mice and are expressed as mean + SEM. **$p < 0.01$ versus saline, *post hoc* test.

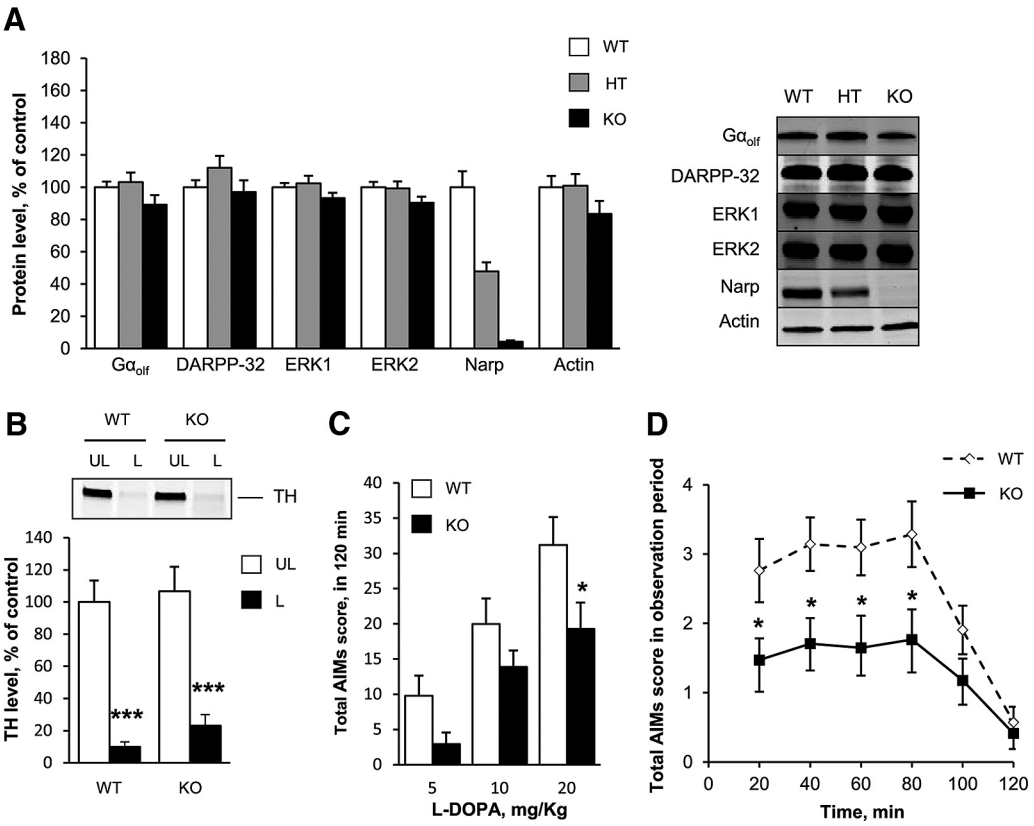

Figure 7. Reduction of L-DOPA-induced dyskinesia in Narp KO mice. ***A***, Protein levels of DARPP-32, Gα_{olf}, ERK1/2, Narp, and actin assessed by immunoblotting in the striatum of WT mice ($n = 12$), homozygous (KO, $n = 11$), and heterozygous (HT, $n = 12$) Narp KO mice. A representative immunoblot (right) is presented. The protein levels of DARPP-32, Gα_{olf}, ERK1/2 and actin (left) were not significantly different between genotypes. Data were normalized on WT mice and correspond to the mean + SEM. ***B***, Comparison of dopamine neuron lesion in Narp KO and WT 6-OHDA-lesioned mice. Dopaminergic fiber lesion was assessed by determining the striatal levels of TH by immunoblotting in the lesioned (L) and unlesioned (UL) striatum of the WT ($n = 21$) and Narp KO ($n = 17$) mice, previously scored for AIMs. A comparable degree of dopamine denervation was observed in both groups. Data are expressed as means + SEM of percentage of the mean in the unlesioned striata (control). ***$p < 0.001$, lesioned versus unlesioned side, *post hoc* test. ***C***, Total AIM score obtained after each period of treatment with L-DOPA at 5, 10, and 20 mg/kg (see Materials and Methods) in 6-OHDA-lesioned WT mice (white boxes, $n = 17$) and Narp KO mice (black boxes, $n = 21$). Total AIM scores are the sum of scores obtained every 20 min for 2 h after L-DOPA treatment. Data are expressed as means + SEM. *$p < 0.05$, KO versus WT, *post hoc* test. ***D***, Time course of AIM score after L-DOPA (20 mg/kg on day 15 of treatment; see Materials and Methods) in WT mice (white boxes, $n = 21$) and Narp KO mice (black boxes, $n = 27$). Data are expressed as means ± SEM. *$p < 0.05$, KO versus WT, *post hoc* test.

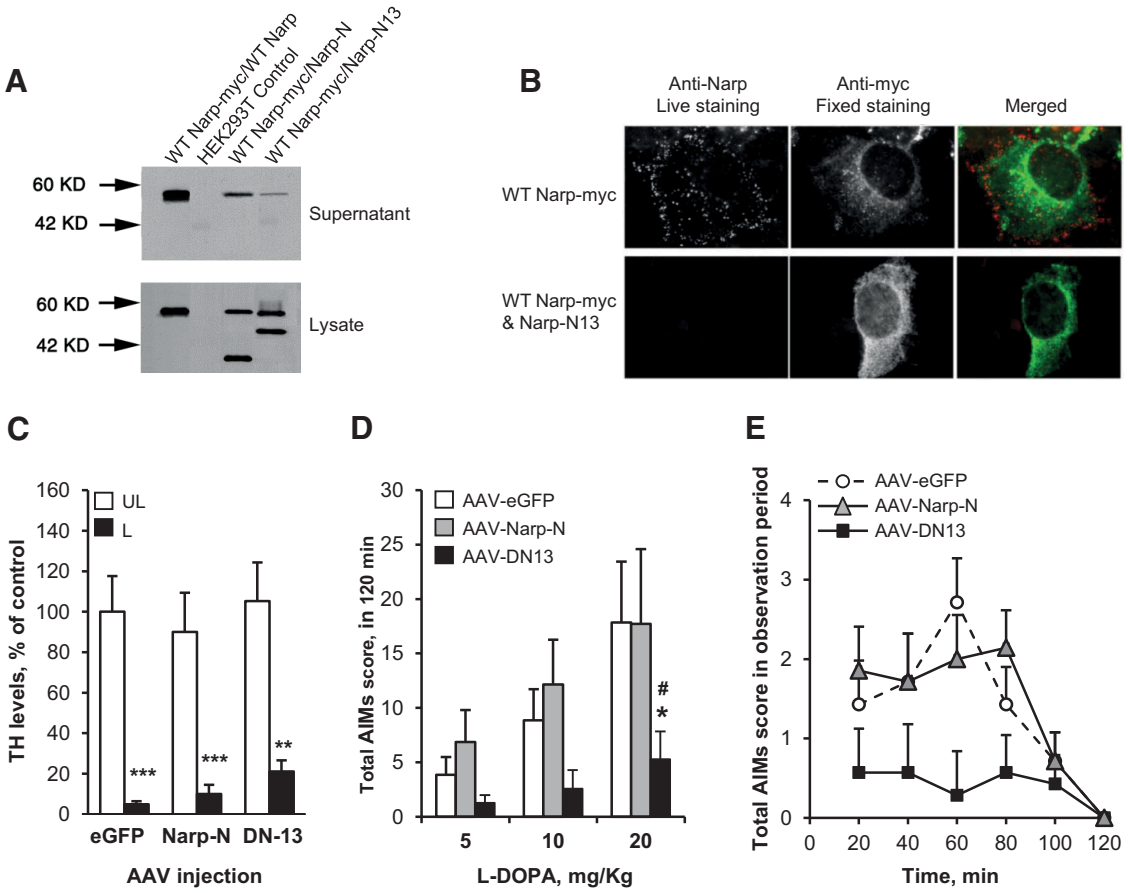

Figure 8. L-DOPA-induced dyskinesia in mice injected with AAV-Narp-N, AAV-DN13, or AAV-GFP in the striatum. Narp deletion constructs act as dominant negatives for secretion of WT Narp. ***A***, Narp constructs were expressed in combination with WT Narp in HEK293 cells and, after 48 h, Narp proteins were examined by Western blot using Narp antibody in supernatant and cell lysate. Mutation within the pentraxin domain (Narp-N13; Δ345–416) prevents its secretion and reduces secretion of coexpressed WT Narp (lane 4). Complete deletion of the pentraxin domain (Narp-N; Δ191–410) did not prevent secretion of coexpressed WT Narp (lane 3). ***B***, Narp-N13 prevents expression of WT Narp on the cell surface of HEK293 cells. Cells expressing the indicated constructs were live labeled with Narp antibody and then fixed and permeabilized and labeled with myc antibody to confirm intracellular expression of WT Narp-myc. ***C–E***, Comparison of mice injected in the striatum with an AAV containing the dominant-negative Narp-N13 (AAV-DN13, $n = 7$), Narp-N (AAV-Narp-N, $n = 7$), or the green fluorescent protein (AAV-eGFP, $n = 7$). ***C***, Dopamine fiber lesion was assessed by determining the striatal levels of TH by immunoblotting in the lesioned (L) and unlesioned (UL) striatum. Values are means + SEM. $^{***}p < 0.001$, $^{**}p < 0.01$, L versus UL side, *post hoc* Newman–Keuls test. ***D***, Total AIMs score obtained after each period of treatment with L-DOPA at 5, 10, and 20 mg/kg. Total AIMs scores are the sum of scores obtained every 20 min for 2 h after L-DOPA. Data are means + SEM. $^{*}p < 0.05$, AAV-DN13 versus AAV-GFP, #$p < 0.05$ AAV-DN13 versus AAV-Narp-N, *post hoc* Newman–Keuls test. ***E***, Time course of AIMs score after L-DOPA at 20 mg/kg (day 15). Values are means ± SEM.

(Andersson et al., 1999; Cenci et al., 1999; Heiman et al., 2014). Several lines of evidence support the role in LID of ΔFosB, a well characterized splice variant product of the *FosB* gene coding for a truncated stable protein. Overexpression of ΔFosB in the dopamine-denervated striatum reproduced abnormal movements when associated with L-DOPA (Cao et al., 2010), whereas overexpression of ΔJunD, a truncated form of JunD, acting as a dominant-negative form of ΔFosB decreased established LID in monkey (Berton et al., 2009). The second gene in our list, *Th*, encodes TH, the enzyme that converts tyrosine into L-DOPA. At first glance, this result may seem surprising because, in the striatum, TH protein levels are dramatically reduced after lesion of dopaminergic terminals. However, previous experiments identified a population of TH-positive neurons in the dopamine-depleted mouse striatum, which increased after L-DOPA treatment (Darmopil et al., 2008). These neurons corresponded to MSNs, in agreement with previous observations (Tashiro et al., 1989) and with a recent study showing increased TH mRNA in D1R-expressing MSNs (Heiman et al., 2014). The number of striatal TH-positive neurons correlates with the level of *FosB* and with the severity of LID in hemiparkinsonian mice (Francardo et al., 2011; Heiman et al., 2014). Our results suggest that TH expression in striatal neurons is regulated in an ERK-dependent manner and may be implicated in the occurrence of LID. *Nedd4l* encodes an E3 ubiquitin protein ligase that mediates the ubiquitination of multiple target substrates (Harvey and Kumar, 1999). Interestingly, recent findings suggest that L-DOPA impairs ubiquitin-proteasome activity in parkinsonism through D1R and may contribute to LID development (Berthet et al., 2012). *Ccrn4l* (CCR4 carbon catabolite repression 4-like) codes for nocturnin, a circadian deadenylase that confers resistance to diet-induced obesity (Green et al., 2007) and the function of which in the brain is not characterized. Interestingly, a recent study found that *Th*, *Nedd4l*, *Ccrn4l*, *Nptx2*, and *FosB* genes are deregulated preferentially in the D1R-expressing MSNs by chronic L-DOPA treatment (Heiman et al., 2014).

We focused on *Nptx2*, the most significantly differently expressed gene between highly and weakly dyskinetic mice after *FosB*. We found that AIMs generated by chronic administration of L-DOPA were significantly reduced in Narp KO mice, making it a prime candidate for the generation of LID. Moreover, expression of a dominant-negative form of Narp dramatically improved

LID in lesioned WT mice. *Nptx2* encodes Narp, a member of the neuronal pentraxin family also including neuronal pentraxin 1 (NP1) and the neuronal pentraxin receptor (NPR). *Nptx2* is an IEG induced by neuronal activation (Tsui et al., 1996) and by D1R stimulation in the striatum of 6-OHDA-lesioned rats (Berke et al., 1998). Narp is a secreted protein that binds to the extracellular surface of AMPARs and regulates their synaptic clustering (O'Brien et al., 2002). In the hippocampus, Narp is enriched at excitatory synapses on parvalbumin interneurons (Chang et al., 2010). Narp and NP1 enhance glutamate signaling by clustering AMPA receptors and NPR mediates endocytosis of surface AMPARs during mGluR1-dependent LTD (Cho et al., 2008). Considering its crucial role in the homeostasis of synaptic plasticity, Narp overexpression after L-DOPA treatment may play a role in LID development by promoting abnormal plasticity of corticostriatal synapses through postsynaptic AMPAR clustering (Kobylecki et al., 2010) and may participate in ERK-dependent dysregulation of striatal synaptic plasticity (Cerovic et al., 2014). Our experiments showing decreased LID intensity in Narp KO mice or after expression of a dominant-negative form of Narp in the striatum support this hypothesis. Interestingly, increased Narp mRNA levels have been reported in the prefrontal cortex and substantia nigra of PD patients, with increased Narp immunoreactivity in Lewy bodies (Moran et al., 2008). Although the relevance of these findings for the development of LID remains to be determined, they may indicate a particular reactivity of Narp expression after dopamine depletion. Narp has also been found to play a role in long-term behavioral alterations associated with chronic stimulation of dopamine transmission, such as cocaine-induced behaviors (Pacchioni, 2009a,2009b). It will be important in future studies to determine how Narp, and possibly other neuronal pentraxin family members, regulate the stability of synaptic plasticity that underlies rapid and long-lasting changes in behavior related to dopamine depletion and L-DOPA therapy.

Our results confirm that a major effect of L-DOPA in the dopamine-depleted striatum is the induction of a molecular signature corresponding to intracellular signaling cascades regulating synaptic plasticity. The acute administration of L-DOPA regulates genes encoding positive and negative regulators of the D1R/PKA/DARPP-32/ERK cascades that most likely result in a global negative feedback, which may explain its progressive downregulation after repeated administration. We identified Narp as a candidate for the early development of LID, suggesting that the homeostasis of glutamate receptors at corticostriatal and/or thalamostriatal synapses is an important element of the maladaptive plasticity that leads to LID. Although extrapolation to human pathology has to be very cautious due to the intrinsic limitation of the animal model used in this study, early molecular events induced during the "induction" phase of L-DOPA treatment, such as Narp secretion, could be attractive targets for therapeutic intervention aimed at preventing LID occurrence in patients with PD.

References

Alcacer C, Santini E, Valjent E, Gaven F, Girault JA, Hervé D (2012) Gα(olf) mutation allows parsing the role of cAMP-dependent and extracellular signal-regulated kinase-dependent signaling in L-3,4-dihydroxyphenylalanine-induced dyskinesia. J Neurosci 32:5900–5910. CrossRef Medline

Andersson M, Hilbertson A, Cenci MA (1999) Striatal fosB expression is causally linked with l-DOPA-induced abnormal involuntary movements and the associated upregulation of striatal prodynorphin mRNA in a rat model of Parkinson's disease. Neurobiol Dis 6:461–474. CrossRef Medline

Andersson M, Westin JE, Cenci MA (2003) Time course of striatal DeltaFosB-like immunoreactivity and prodynorphin mRNA levels after discontinuation of chronic dopaminomimetic treatment. Eur J Neurosci 17:661–666. CrossRef Medline

Aubert I, Guigoni C, Håkansson K, Li Q, Dovero S, Barthe N, Bioulac BH, Gross CE, Fisone G, Bloch B, Bezard E (2005) Increased D1 dopamine receptor signaling in levodopa-induced dyskinesia. Ann Neurol 57:17–26. CrossRef Medline

Bateup HS, Santini E, Shen W, Birnbaum S, Valjent E, Surmeier DJ, Fisone G, Nestler EJ, Greengard P (2010) Distinct subclasses of medium spiny neurons differentially regulate striatal motor behaviors. Proc Natl Acad Sci U S A 107:14845–14850. CrossRef Medline

Berke JD, Paletzki RF, Aronson GJ, Hyman SE, Gerfen CR (1998) A complex program of striatal gene expression induced by dopaminergic stimulation. J Neurosci 18:5301–5310. Medline

Berthet A, Bezard E, Porras G, Fasano S, Barroso-Chinea P, Dehay B, Martinez A, Thiolat ML, Nosten-Bertrand M, Giros B, Baufreton J, Li Q, Bloch B, Martin-Negrier ML (2012) L-DOPA impairs proteasome activity in parkinsonism through D1 dopamine receptor. J Neurosci 32:681–691. CrossRef Medline

Berton O, Guigoni C, Li Q, Bioulac BH, Aubert I, Gross CE, Dileone RJ, Nestler EJ, Bezard E (2009) Striatal overexpression of DeltaJunD resets L-DOPA-induced dyskinesia in a primate model of Parkinson disease. Biol Psychiatry 66:554–561. CrossRef Medline

Bjartmar L, Huberman AD, Ullian EM, Rentería RC, Liu X, Xu W, Prezioso J, Susman MW, Stellwagen D, Stokes CC, Cho R, Worley P, Malenka RC, Ball S, Peachey NS, Copenhagen D, Chapman B, Nakamoto M, Barres BA, Perin MS (2006) Neuronal pentraxins mediate synaptic refinement in the developing visual system. J Neurosci 26:6269–6281. CrossRef Medline

Calabresi P, Gubellini P, Centonze D, Picconi B, Bernardi G, Chergui K, Svenningsson P, Fienberg AA, Greengard P (2000) Dopamine and cAMP-regulated phosphoprotein 32 kDa controls both striatal long-term depression and long-term potentiation, opposing forms of synaptic plasticity. J Neurosci 20:8443–8451. Medline

Calabresi P, Picconi B, Tozzi A, Di Filippo M (2007) Dopamine-mediated regulation of corticostriatal synaptic plasticity. Trends Neurosci 30:211–219. CrossRef Medline

Calon F, Hadj Tahar A, Blanchet PJ, Morissette M, Grondin R, Goulet M, Doucet JP, Robertson GS, Nestler E, Di Paolo T, Bédard PJ (2000) Dopamine-receptor stimulation: biobehavioral and biochemical consequences. Trends Neurosci 23:S92–S100. CrossRef Medline

Cao X, Yasuda T, Uthayathas S, Watts RL, Mouradian MM, Mochizuki H, Papa SM (2010) Striatal overexpression of DeltaFosB reproduces chronic levodopa-induced involuntary movements. J Neurosci 30:7335–7343. CrossRef Medline

Cenci MA, Konradi C (2010) Maladaptive striatal plasticity in L-DOPA-induced dyskinesia. Prog Brain Res 183:209–233. CrossRef Medline

Cenci MA, Tranberg A, Andersson M, Hilbertson A (1999) Changes in the regional and compartmental distribution of FosB- and JunB-like immunoreactivity induced in the dopamine-denervated rat striatum by acute or chronic L-DOPA treatment. Neuroscience 94:515–527. CrossRef Medline

Cerovic M, Bagetta V, Pendolino V, Ghiglieri V, Fasano S, Morella I, Hardingham N, Heuer A, Papale A, Marchisella F, Giampà C, Calabresi P, Picconi B, Brambilla R (2014) Derangement of Ras-guanine nucleotide-releasing factor 1 (Ras-GRF1) and extracellular signal-regulated kinase (ERK) dependent striatal plasticity in L-DOPA-induced dyskinesia. Biol Psychiatry. Advance online publication. doi:10.1016/j.biopsych.2014.04.002. CrossRef Medline

Chang MC, Park JM, Pelkey KA, Grabenstatter HL, Xu D, Linden DJ, Sutula TP, McBain CJ, Worley PF (2010) Narp regulates homeostatic scaling of excitatory synapses on parvalbumin-expressing interneurons. Nat Neurosci 13:1090–1097. CrossRef Medline

Cho RW, Park JM, Wolff SB, Xu D, Hopf C, Kim JA, Reddy RC, Petralia RS, Perin MS, Linden DJ, Worley PF (2008) mGluR1/5-dependent long-term depression requires the regulated ectodomain cleavage of neuronal pentraxin NPR by TACE. Neuron 57:858–871. CrossRef Medline

Corvol JC, Muriel MP, Valjent E, Féger J, Hanoun N, Girault JA, Hirsch EC, Hervé D (2004) Persistent increase in olfactory type G-protein alpha subunit levels may underlie D1 receptor functional hypersensitivity in Parkinson disease. J Neurosci 24:7007–7014. CrossRef Medline

Darmopil S, Muñetón-Gómez VC, de Ceballos ML, Bernson M, Moratalla R (2008) Tyrosine hydroxylase cells appearing in the mouse striatum after

dopamine denervation are likely to be projection neurones regulated by L-DOPA. Eur J Neurosci 27:580–592. CrossRef Medline

Darmopil S, Martín AB, De Diego IR, Ares S, Moratalla R (2009) Genetic inactivation of dopamine D1 but not D2 receptors inhibits L-DOPA-induced dyskinesia and histone activation. Biol Psychiatry 66:603–613. CrossRef Medline

Ding Y, Won L, Britt JP, Lim SA, McGehee DS, Kang UJ (2011) Enhanced striatal cholinergic neuronal activity mediates L-DOPA-induced dyskinesia in parkinsonian mice. Proc Natl Acad Sci U S A 108:840–845. CrossRef Medline

During MJ, Young D, Baer K, Lawlor P, Klugmann M (2003) Development and optimization of adeno-asssociated virus vector transfer into the central nervous system. Methods Mol Med 76:221–236. Medline

Duvoisin RC (1974) Variations in the "on-off" phenomenon. Adv Neurol 5:339–340. Medline

El Atifi-Borel M, Buggia-Prevot V, Platet N, Benabid AL, Berger F, Sgambato-Faure V (2009) De novo and long-term l-Dopa induce both common and distinct striatal gene profiles in the hemiparkinsonian rat. Neurobiol Dis 34:340–350. CrossRef Medline

Fasano S, Bezard E, D'Antoni A, Francardo V, Indrigo M, Qin L, Doveró S, Cerovic M, Cenci MA, Brambilla R (2010) Inhibition of Ras-guanine nucleotide-releasing factor 1 (Ras-GRF1) signaling in the striatum reverts motor symptoms associated with L-DOPA-induced dyskinesia. Proc Natl Acad Sci U S A 107:21824–21829. CrossRef Medline

Francardo V, Recchia A, Popovic N, Andersson D, Nissbrandt H, Cenci MA (2011) Impact of the lesion procedure on the profiles of motor impairment and molecular responsiveness to L-DOPA in the 6-hydroxydopamine mouse model of Parkinson's disease. Neurobiol Dis 42:327–340. CrossRef Medline

Gerfen CR, Engber TM, Mahan LC, Susel Z, Chase TN, Monsma FJ Jr, Sibley DR (1990) D1 and D2 dopamine receptor-regulated gene expression of striatonigral and striatopallidal neurons. Science 250:1429–1432. CrossRef Medline

Gerfen CR, Miyachi S, Paletzki R, Brown P (2002) D1 dopamine receptor supersensitivity in the dopamine-depleted striatum results from a switch in the regulation of ERK1/2/MAP kinase. J Neurosci 22:5042–5054. Medline

Gerfen CR, Paletzki R, Worley P (2008) Differences between dorsal and ventral striatum in Drd1a dopamine receptor coupling of dopamine- and cAMP-regulated phosphoprotein-32 to activation of extracellular signal-regulated kinase. J Neurosci 28:7113–7120. CrossRef Medline

Green CB, Douris N, Kojima S, Strayer CA, Fogerty J, Lourim D, Keller SR, Besharse JC (2007) Nocturnin, a circadian deadenylase, confers resistance to hepatic steatosis and diet-induced obesity. Proc Natl Acad Sci U S A 104:9888–9893. CrossRef Medline

Harvey KF, Kumar S (1999) Nedd4-like proteins: an emerging family of ubiquitin-protein ligases implicated in diverse cellular functions. Trends Cell Biol 9:166–169. CrossRef Medline

Heiman M, Heilbut A, Francardo V, Kulicke R, Fenster RJ, Kolaczyk ED, Mesirov JP, Surmeier DJ, Cenci MA, Greengard P (2014) Molecular adaptations of striatal spiny projection neurons during levodopa-induced dyskinesia. Proc Natl Acad Sci U S A 111:4578–4583. CrossRef Medline

Hervé D, Lévi-Strauss M, Marey-Semper I, Verney C, Tassin JP, Glowinski J, Girault JA (1993) G(olf) and Gs in rat basal ganglia: possible involvement of G(olf) in the coupling of dopamine D1 receptor with adenylyl cyclase. J Neurosci 13:2237–2248. Medline

Huang da W, Sherman BT, Lempicki RA (2009a) Systematic and integrative analysis of large gene lists using DAVID Bioinformatics Resources. Nat Protoc 4:44–57. Medline

Huang da W, Sherman BT, Lempicki RA (2009b) Bioinformatics enrichment tools: paths toward the comprehensive functional analysis of large gene lists. Nucleic Acids Res 37:1–13. CrossRef Medline

Huot P, Lévesque M, Parent A (2007) The fate of striatal dopaminergic neurons in Parkinson's disease and Huntington's chorea. Brain 130:222–232. CrossRef Medline

Jenner P (2008) Molecular mechanisms of L-DOPA-induced dyskinesia. Nat Rev Neurosci 9:665–677. CrossRef Medline

Kobylecki C, Cenci MA, Crossman AR, Ravenscroft P (2010) Calcium-permeable AMPA receptors are involved in the induction and expression of l-DOPA-induced dyskinesia in Parkinson's disease. J Neurochem 114:499–511. CrossRef Medline

Kreitzer AC, Malenka RC (2007) Endocannabinoid-mediated rescue of striatal LTD and motor deficits in Parkinson's disease models. Nature 445:643–647. CrossRef Medline

Lebel M, Chagniel L, Bureau G, Cyr M (2010) Striatal inhibition of PKA prevents levodopa-induced behavioural and molecular changes in the hemiparkinsonian rat. Neurobiol Dis 38:59–67. CrossRef Medline

Lindgren HS, Ohlin KE, Cenci MA (2009) Differential involvement of D1 and D2 dopamine receptors in L-DOPA-induced angiogenic activity in a rat model of Parkinson's disease. Neuropsychopharmacology 34:2477–2488. CrossRef Medline

Lundblad M, Andersson M, Winkler C, Kirik D, Wierup N, Cenci MA (2002) Pharmacological validation of behavioural measures of akinesia and dyskinesia in a rat model of Parkinson's disease. Eur J Neurosci 15:120–132. CrossRef Medline

Lundblad M, Picconi B, Lindgren H, Cenci MA (2004) A model of L-DOPA-induced dyskinesia in 6-hydroxydopamine lesioned mice: relation to motor and cellular parameters of nigrostriatal function. Neurobiol Dis 16:110–123. CrossRef Medline

Lundblad M, Usiello A, Carta M, Håkansson K, Fisone G, Cenci MA (2005) Pharmacological validation of a mouse model of l-DOPA-induced dyskinesia. Exp Neurol 194:66–75. CrossRef Medline

Meurers BH, Dziewczapolski G, Shi T, Bittner A, Kamme F, Shults CW (2009) Dopamine depletion induces distinct compensatory gene expression changes in DARPP-32 signal transduction cascades of striatonigral and striatopallidal neurons. J Neurosci 29:6828–6839. CrossRef Medline

Moran LB, Hickey L, Michael GJ, Derkacs M, Christian LM, Kalaitzakis ME, Pearce RK, Graeber MB (2008) Neuronal pentraxin II is highly upregulated in Parkinson's disease and a novel component of Lewy bodies. Acta Neuropathol 115:471–478. CrossRef Medline

Nadjar A, Gerfen CR, Bezard E (2009) Priming for L-DOPA-induced dyskinesia in Parkinson's disease: a feature inherent to the treatment or the disease? Prog Neurobiol 87:1–9. CrossRef Medline

Obeso JA, Rodriguez-Oroz MC, Rodriguez M, DeLong MR, Olanow CW (2000) Pathophysiology of levodopa-induced dyskinesias in Parkinson's disease: problems with the current model. Ann Neurol 47:S22–S32; discussion S32–S34. Medline

O'Brien R, Xu D, Mi R, Tang X, Hopf C, Worley P (2002) Synaptically targeted Narp plays an essential role in the aggregation of AMPA receptors at excitatory synapses in cultured spinal neurons. J Neurosci 22:4487–4498. Medline

Pacchioni AM, Kalivas PW (2009a) The role of AMPAR trafficking mediated by neuronal pentraxins in cocaine-induced neuroadaptations. Mol Cell Pharmacol 1:183–192. CrossRef Medline

Pacchioni AM, Vallone J, Worley PF, Kalivas PW (2009b) Neuronal pentraxins modulate cocaine-induced neuroadaptations. J Pharmacol Exp Ther 328:183–192. CrossRef Medline

Pavón N, Martín AB, Mendialdua A, Moratalla R (2006) ERK phosphorylation and FosB expression are associated with L-DOPA-induced dyskinesia in hemiparkinsonian mice. Biol Psychiatry 59:64–74. CrossRef Medline

Paxinos G, Franklin KBJ (2001) The mouse brain in stereotaxic coordinates, Ed 2. San Diego: Academic.

Picconi B, Centonze D, Håkansson K, Bernardi G, Greengard P, Fisone G, Cenci MA, Calabresi P (2003) Loss of bidirectional striatal synaptic plasticity in L-DOPA-induced dyskinesia. Nat Neurosci 6:501–506. CrossRef Medline

Putterman DB, Munhall AC, Kozell LB, Belknap JK, Johnson SW (2007) Evaluation of levodopa dose and magnitude of dopamine depletion as risk factors for levodopa-induced dyskinesia in a rat model of Parkinson's disease. J Pharmacol Exp Ther 323:277–284. CrossRef Medline

Rangel-Barajas C, Silva I, Lopéz-Santiago LM, Aceves J, Erlij D, Florán B (2011) L-DOPA-induced dyskinesia in hemiparkinsonian rats is associated with up-regulation of adenylyl cyclase type V/VI and increased GABA release in the substantia nigra reticulata. Neurobiol Dis 41:51–61. CrossRef Medline

Saeed AI, Sharov V, White J, Li J, Liang W, Bhagabati N, Braisted J, Klapa M, Currier T, Thiagarajan M, Sturn A, Snuffin M, Rezantsev A, Popov D, Ryltsov A, Kostukovich E, Borisovsky I, Liu Z, Vinsavich A, Trush V, Quackenbush J (2003) TM4: a free, open-source system for microarray data management and analysis. Biotechniques 34:374–378. Medline

Santini E, Valjent E, Usiello A, Carta M, Borgkvist A, Girault JA, Hervé D, Greengard P, Fisone G (2007) Critical involvement of cAMP/DARPP-32 and extracellular signal-regulated protein kinase signaling in L-DOPA-induced dyskinesia. J Neurosci 27:6995–7005. CrossRef Medline

Santini E, Alcacer C, Cacciatore S, Heiman M, Hervé D, Greengard P, Girault JA, Valjent E, Fisone G (2009a) L-DOPA activates ERK signaling and phosphorylates histone H3 in the striatonigral medium spiny neurons of hemiparkinsonian mice. J Neurochem 108:621–633. CrossRef Medline

Santini E, Heiman M, Greengard P, Valjent E, Fisone G (2009b) Inhibition of mTOR signaling in Parkinson's disease prevents L-DOPA-induced dyskinesia. Sci Signal 2:ra36. CrossRef Medline

Santini E, Sgambato-Faure V, Li Q, Savasta M, Dovero S, Fisone G, Bezard E (2010) Distinct changes in cAMP and extracellular signal-regulated protein kinase signalling in L-DOPA-induced dyskinesia. PLoS One 5:e12322. CrossRef Medline

Santini E, Feyder M, Gangarossa G, Bateup HS, Greengard P, Fisone G (2012) Dopamine-and cAMP-regulated phosphoprotein of 32-kDa (DARPP-32)-dependent activation of extracellular signal-regulated kinase (ERK) and mammalian target of rapamycin complex 1 (mTORC1) signaling in experimental parkinsonism. J Biol Chem 287:27806–27812. CrossRef Medline

Schuster S, Nadjar A, Guo JT, Li Q, Ittrich C, Hengerer B, Bezard E (2008) The 3-hydroxy-3-methylglutaryl-CoA reductase inhibitor lovastatin reduces severity of L-DOPA-induced abnormal involuntary movements in experimental Parkinson's disease. J Neurosci 28:4311–4316. CrossRef Medline

Shen W, Flajolet M, Greengard P, Surmeier DJ (2008) Dichotomous dopaminergic control of striatal synaptic plasticity. Science 321:848–851. CrossRef Medline

Tashiro Y, Sugimoto T, Hattori T, Uemura Y, Nagatsu I, Kikuchi H, Mizuno N (1989) Tyrosine hydroxylase-like immunoreactive neurons in the striatum of the rat. Neurosci Lett 97:6–10. CrossRef Medline

Tsui CC, Copeland NG, Gilbert DJ, Jenkins NA, Barnes C, Worley PF (1996) Narp, a novel member of the pentraxin family, promotes neurite outgrowth and is dynamically regulated by neuronal activity. J Neurosci 16:2463–2478. Medline

Valjent E, Pascoli V, Svenningsson P, Paul S, Enslen H, Corvol JC, Stipanovich A, Caboche J, Lombroso PJ, Nairn AC, Greengard P, Hervé D, Girault JA (2005) Regulation of a protein phosphatase cascade allows convergent dopamine and glutamate signals to activate ERK in the striatum. Proc Natl Acad Sci U S A 102:491–496. CrossRef Medline

Westin JE, Vercammen L, Strome EM, Konradi C, Cenci MA (2007) Spatiotemporal pattern of striatal ERK1/2 phosphorylation in a rat model of L-DOPA-induced dyskinesia and the role of dopamine D1 receptors. Biol Psychiatry 62:800–810. CrossRef Medline

Xu D, Hopf C, Reddy R, Cho RW, Guo L, Lanahan A, Petralia RS, Wenthold RJ, O'Brien RJ, Worley P (2003) Narp and NP1 form heterocomplexes that function in developmental and activity-dependent synaptic plasticity. Neuron 39:513–528. Medline